Exploring implications of input parameter uncertainties on GLOF modelling results using the ~~state-of-the-art~~ modelling code~~,~~ r.avaflow

Sonam Rinzin[1], Stuart Dunning[1], Rachel Joanne Carr[1], Ashim Sattar[2], Martin Mergili[3]

[1]School of Geography, Politics and Sociology, Newcastle University, United Kingdom

[2]~~Divecha Centre for Climate Change, Indian Institute of Science, India~~Indian Institute of Technology Bhubaneswar

[3]~~Institute~~ [3]Department of Geography and Regional Science, University of Graz, Austria

Correspondence to: Sonam Rinzin at s.rinzin2@newcastle.ac.uk

Abstract

Modelling complex mass flow processes, such as glacial lake outburst floods (GLOFs), for hazard and risk assessments requires extensive data and computational resources. Researchers often rely on low-resolution, open-access datasets and parameters derived from plausibility due to the difficulty involved in conducting direct measurements. ~~As a result, it introduces c~~This results in considerable uncertainties in forward modelling, potentially limiting the accuracy and reliability of predictions. ~~Modelling complex mass flow processes like glacial lake outburst floods (GLOFs) for hazard and risk assessments involves substantial data and computational resources, often leading researchers to use low-resolution, open-access data and parameters based on plausibility rather than direct measurement, which, although effective in back analysis, introduces significant uncertainties in forward modelling.~~ To determine the sensitivity of the model outputs stemming from input parameter uncertainties in the forward modelling, we selected nine parameters relevant to GLOF modelling and performed a total of ~~78~~ 84 ~~s~~simulations each representing a unique GLOF scenario in the physically-based r.avaflow model. Our results indicate that mass movement-triggered moraine-dammed GLOF modelling outputs are notably sensitive to ~~six~~ five parameters, which are, in order of importance: 1) volume of mass movements entering lakes; 2) DEM datasets; 3) the origin of mass movements; 4) ~~mesh size~~Eentrainment coefficient; and 5) basal frictional angle~~; and 6) entrainment coefficient~~. The GLOF output parameter resulting from ~~T~~the volume of mass movement impacting lakes has the greatest ~~impact on GLOF output, with an average~~ coefficient of variation (CV) = 47%, while the internal friction angle had the least ~~impact (~~CV (=0.4%). We recommend that future GLOF modelling should carefully consider the output uncertainty stemming from the sensitive input parameters identified here, some of which cannot be constrained before a GLOF and ~~and~~ must be addressed using statistical approaches~~must be considered only statistically~~.

1 Introduction

Glacial lakes can store millions of cubic meters of (Zhang et al., 2024; Zhang et al., 2023a; Shugar et al., 2020)~~water~~: as of ~~2015~~2020, it is estimated that glacial lakes (0.002 km^2) ~~(>=0.05 km^2)~~ store about 1280.6 ± 354.1 km^3 ~~≈105.7 km^3~~ of water ~~(Shugar et al., 2020)~~ in the world (Zhang et al., 2024)~~globally (Zhang et al., 2023a; Shugar et al., 2020; Zheng et al., 2021b)~~. The ~~Although g~~glacial lakes in High Mountain Asia (HMA) ~~contribute only 4.6 km^3 to this total volume, they~~ have experienced the greatest expansion (46%) between 1990 and 2018 (Shugar et al., 2020). Furthermore, over 28% of glacial lakes in ~~the~~ HMA are dammed by loose/destabilizing moraines (Fujita et al., 2013; Zheng et al., 2021b) and the majority of glacial lakes (70%) are exposed to ~~mass inputssteep~~mass inputs ~~slopes,~~ in the form of ice/snow avalanches, rockfalls and landslides from the surrounding slopes (Dubey et al., 2023). ~~Although there is no substantial evidence for an increasing trend in glacial lake outburst floods (GLOF) within existing data (between 850 and 2022 CE) (Shrestha et al., 2023; Lützow et al., 2023; Veh et al., 2022; Veh et al., 2023), the GLOF frequency is expected to increase in the future (Zheng et al., 2021) because the glaciers and permafrost in HMA are extremely sensitive to rising temperatures (Gruber et al., 2017; Kääb et al., 2018).~~ Meltwater resulting from the shrinkage of glaciers leads to the formation of new glacial lakes and the expansion of existing ones (Zhang et al., 2015; Wang et al., 2020). This process sometimes exposes them to mass movement from the slopes above and increases the total volume of stored water (Rounce et al., 2016). Additionally, the degradation of permafrost destabilizes the slopes surrounding the glacial lakes, increasing the likelihood of mass movements into lakes (Huggel, 2009).

Recent work has documented 3151 GLOF events between 850 and 2022 C.E. globally (Lützow et al., 2023) and 682 GLOF events in HMA between 1833 and 2022 (Shrestha et al., 2023). In ~~the~~ HMA alone, these GLOF events have resulted in 6907 human deaths, caused damage to more than 2200 buildings, 71 km^2 of agricultural land, 163 MW capacity of hydropower, 2000 livestock and numerous other structures, including bridges and roads (Shrestha et al., 2023). However, these reported deaths and damages are significantly underestimated because of patchy documentation (Carrivick and Tweed, 2016). ~~Unfortunately, t~~The risk from GLOF is expected to rise in the future with the anticipated expansion of glacial lakes (Zheng et al., 2021b; Zhang et al., 2023b) compounded by a growing population and the construction of structures in areas prone to GLOFs (Taylor et al., 2023; Nie et al., 2023).

Most GLOF events in HMA start with mass movements entering the lake from surrounding slopes, leading to the displacement of water and waves overtopping the dam (Shrestha et al., 2023; Lützow et al., 2023; Nie et al., 2018). ~~The m~~Mass movements such as ~~R~~ rock- or ice-

avalanches and landslides entering the lake constitute 70% of known causes of HMA historical GLOF events (Shrestha et al., 2023). The overtopping waves cause moraine dam incision and dam failure, resulting in a sudden discharge of lake water. To a lesser extent, GLOF events are also triggered by factors such as ~~increased~~ excess hydrostatic pressure from runoff snow and ice melt, intense rainfall and cloud outbursts, and dam settling caused by the melting of ice cores or internal piping. However, it is important to note that in some cases, these triggering factors may not necessarily result in a complete moraine dam failure~~.~~. As the flood propagates further downstream, it can transform into a debris flow and/ or a hyper-concentrated flow ~~/debris flood~~ depending on the geologic and topographic characteristics of the river channel as well as depending on the ~~-~~availability of erodible sediment and its grain size distribution (Gaphaz, 2017; Schneider et al., 2014; Westoby et al., 2015; Westoby et al., 2014). These complex GLOF process chains are difficult to accurately capture in numerical models, given the large number of processes and parameters~~, and the phase transformations during the event~~, which limits our ability to model the impacts of the hazard cascade as a whole.

1.1 Numerical modelling of GLOFs

Previous studies have used various modelling codes such as HEC-RAS (Sattar et al., 2021b), BASEMENT (Worni et al., 2013; Worni et al., 2012; Byers et al., 2018), FLO-2D (Somos-Valenzuela et al., 2015), RAMMS (Lala et al., 2018), and r.avaflow (Mergili et al., 2020b). Most ~~all~~ of these ~~models~~codes, however, cannot model the evolution of the GLOF process chain through interaction at the boundary of different processes involved (e.g. the interaction of mass movements with the lake) and dynamic transformation of flow through sediment entrainment and deposition. To address this limitation, some of the studies modelled each component separately and then fed the results of each modelling component into the next stage (Lala et al., 2018; Schneider et al., 2014; Frey et al., 2018). For example, Lala et al (2018) have used RAMMS to model mass movement from the surrounding slope into the ~~I~~Imja Lake, Nepal~~ake~~, Heller–Hager and BASEMENT to model wave propagation across the lake surface and BASEMENT to model the subsequent downstream hydrodynamic evolution of GLOF. In contrast, the r.avaflow model (Mergili et al., 2017; Mergili and Pudasaini, 2024~~b~~) enables the integration of all components of the GLOF process chain and their interactions and transformation without the need to combine the results of different models. It enables the detailed modelling of the GLOF process chain, covering everything from the initial trigger to the downstream propagation. r.avaflow is an open-source, GIS-based tool for simulating mass flows over arbitrary terrain. Furthermore, r.avaflow ~~is open source and~~ allows modification of all input parameters, which sets it apart from many modelling codes (where most of the

parameters remain hidden within a 'black box'), making it suitable for conducting GLOF parameter sensitivity analysis (Mergili et al., 2017; Mergili and Pudasaini, 2024~~b~~).

r.avaflow utilizes the total variation diminishing non-oscillatory central differencing (NOC-TVD) numerical scheme (Wang et al., 2004) to solve an enhanced version of the Pudasaini multi-phase flow model (Pudasaini and Mergili, 2019). It also offers added features for entrainment, deposition, dispersion, and phase transformation. Because of these features, r.avaflow can model the full process chain of a GLOF and flow transformation due to erosion of bed material and deposition of entrained material (Mergili et al., 2017; Mergili and Pudasaini, 2024~~b~~). However, the precision of this model output parameters such as peak flow, depth and velocity depends on the accuracy of various input parameters and initial conditions, including the release height of mass, the resolution and vertical accuracy of the digital elevation model (DEM), density, entrainment, and frictional parameters (Mergili et al., 2017). ~~The difficulty involved in getting accurate measurements of these parameters introduces substantial uncertainty in the modelling results.~~

Because of the significant logistic challenges associated with collecting field data and the financial costs involved in acquiring high-resolution remote sensing data, many of the parameters in GLOF modelling are derived from open-access data, leading to considerable uncertainties in the resultant discharge, inundation extent, and arrival times. Also, certain input parameters~~factors~~ such as the volume of mass movement entering the lake are impossible to measure accurately before a GLOF event. For example, the global-scale DEM, SRTM-GL1, with a ground resolution of 30 m, is commonly employed in GLOF modelling without adequately considering the inherent uncertainty due to horizontal and vertical inaccuracies in this DEM (Rinzin et al., 2023). Similarly, the origin of avalanches and other mass movements is determined using low to medium-resolution remote sensing imagery and DEM, often supplemented by secondary datasets like permafrost data (Obu et al., 2019), which can introduce notable uncertainties (Sattar et al., 2023; Allen et al., 2016). When estimating the volume of avalanches entering lakes, DEM differencing between pre- and post-event conditions can be advantageous for reconstructing historical events (Baggio et al., 2021; Zheng et al., 2021a), although the accuracy is contingent upon the vertical and horizontal accuracy and resolution of the data, and the temporal interval between data acquisition~~accusation~~. Likewise, when ice is considered the sole source of the ~~avalanches~~mass movement, ice thickness is employed to calculate the avalanche volume (Allen et al., 2022), for which the accuracy of computed volume relies on the resolution and availability of ice thickness data from the ice-flow inversion model ~~data~~ in the region of interest. Under ~~the~~ circumstances when the depths of landslides and avalanches are not known,

~~conservative~~ arbitrary thicknesses of 10, 30, and 50 m based on past events (Dubey et al., 2023) are often utilised for forward modelling, further contributing to significant uncertainties in the modelling results (Rounce et al., 2017; Rounce et al., 2016; Dubey and Goyal, 2020).

Moreover, the flow parameters in r.avaflow are adjusted and optimised based on the fit of the model's results to well-documented past events (Mergili et al., 2017; Mergili et al., 2020a; Vilca et al., 2021) and the physically plausible range suggested by Mergili et al. (2017), Mergili et al. (2018b) and Mergili et al. (2018a). Efforts to fine-tune parameters to fit with historical events of varying magnitude, temporality and spatiality have led to the use of wide-ranging values. For example, Mergili et al. (2020b) used an internal solid friction angle of 28° to reconstruct the 1941 GLOF process chain of Lake Palcacocha in the Cordillera Blanka, Peru. In contrast, Vilca et al. (2021) used 45° to model the 2020 glacial lake outburst process chain of Lake Salkantycocha located in Cordillera Vilcabamba of Peru. Likewise, the value of the basal friction angle ranges between 6-18° (Baggio et al., 2021; Mergili et al., 2020a) (Supplementary Figure 1 (Fig. S1)). Because each GLOF event is inherently distinct, even when originating from the same glacial lake (Emmer and Cochachine, 2013; Lala et al., 2018), ~~employing~~ inferring reconstructed values from past events for forward modelling introduces substantial uncertainties (Gaphaz, 2017; Mergili et al., 2020b). Finally, r.avaflow model outputs are extremely sensitive to parameters like entrainment coefficient value, basal friction angle and initial release volume (Mergili et al., 2018b; Mergili et al., 2018a; Baggio et al., 2021). ~~However, to our knowledge, how changes in the values of these input parameters affect the model output (for example, peak and total flow, flow depth, flow velocity and arrival time) is not known.~~ While all these indicate that the value of input parameters is highly variable depending on specific events, ~~However,~~ to our knowledge, how changes in the values of these input parameters affect the model output (for example, peak and total flow, flow depth, flow velocity and arrival time) is not known.

To determine the relative contribution of uncertainties in different input parameters to variability in GLOF extent, we identified nine out of 38 input parameters and initial conditions relevant to GLOF flow modelling ~~that have been previously identified as the most important in the literature~~: digital elevation model; ~~mesh size;~~ the volume of mass movement impacting the lake; the origin of mass movement impacting the lake; grain density of mass movement impacting the lake; volume of lake; entrainment coefficient; internal friction angle; basal friction angle; and, fluid friction number (Table S1). Our selection was motivated by the recognition that these input parameters are considered essential and have been frequently adjusted in previous studies to align with values inferred from observed past (Baggio et al., 2021; Mergili et al., 2018b; Allen et al., 2022; Zheng et al., 2021a; Vilca et al., 2021). We believe that these

parameters are the most likely to influence the results of future modelling efforts, making it critical to evaluate their impacts on model outputs. We assessed the sensitivity of the model output to each of these parameters by conducting up to 10 r.avaflow simulations per parameter and varying their values within the range determined from the literature that employed r.avaflow modelling (Fig. S1). We investigated the impact of variation in these parameter values on the model outputs and used the following diagnostic variables: peak discharge; total discharge; flow arrival time; ~~flow height~~flow depth; flow velocity and reach distance. We then calculated the coefficient of variation for each parameter and ranked them based on this metric.

2 Study site

Here, our sensitivity analysis ~~is~~ was conducted on Thorthormi Tsho located at 28.10° N, 90.27° E in the Lunana region of the Bhutan Himalaya (Fig. 1). The area of Thorthormi Tsho has expanded by ~192% since 1990, evolving into the largest proglacial lake (area = 4.35 km^2) in Bhutan by 2020 (Rinzin et al., 2023) (Fig. 1B and 1E). Although the lake level was lowered by 5m by artificially draining out the water between 2008 and 2012 (Nchm, 2019a), Thorthormi Tsho is marked as the most dangerous glacial lake as it is determined to be susceptible to triggering factors (like mass movement entering lake) and potentially unstable moraine damming the lake (Nchm, 2019a; Rinzin et al., 2021) (Fig. 1B). In recent years, Thorthormi Tsho has produced two GLOF events (Nchm, 2023); the first one occurred on June 20, 2019 (Nchm, 2019b), the latest on October 30, 2023. Also, modelling of future predicted GLOF from Thorthormi Tsho shows it can produce a flood with flow volume up to 3~~00~~ × 10^{8}~~^{6}~~ m^3 of water with a peak discharge of up to 75000 m^3 s^{-1}, affecting more than 16000 people and various infrastructures downstream of this glacial lake (Rinzin et al., 2023). This high outburst susceptibility and ~~potential~~ hazard make Thorthormi Tsho an ideal candidate for GLOF modelling to improve our modelling output GLOF uncertainty.

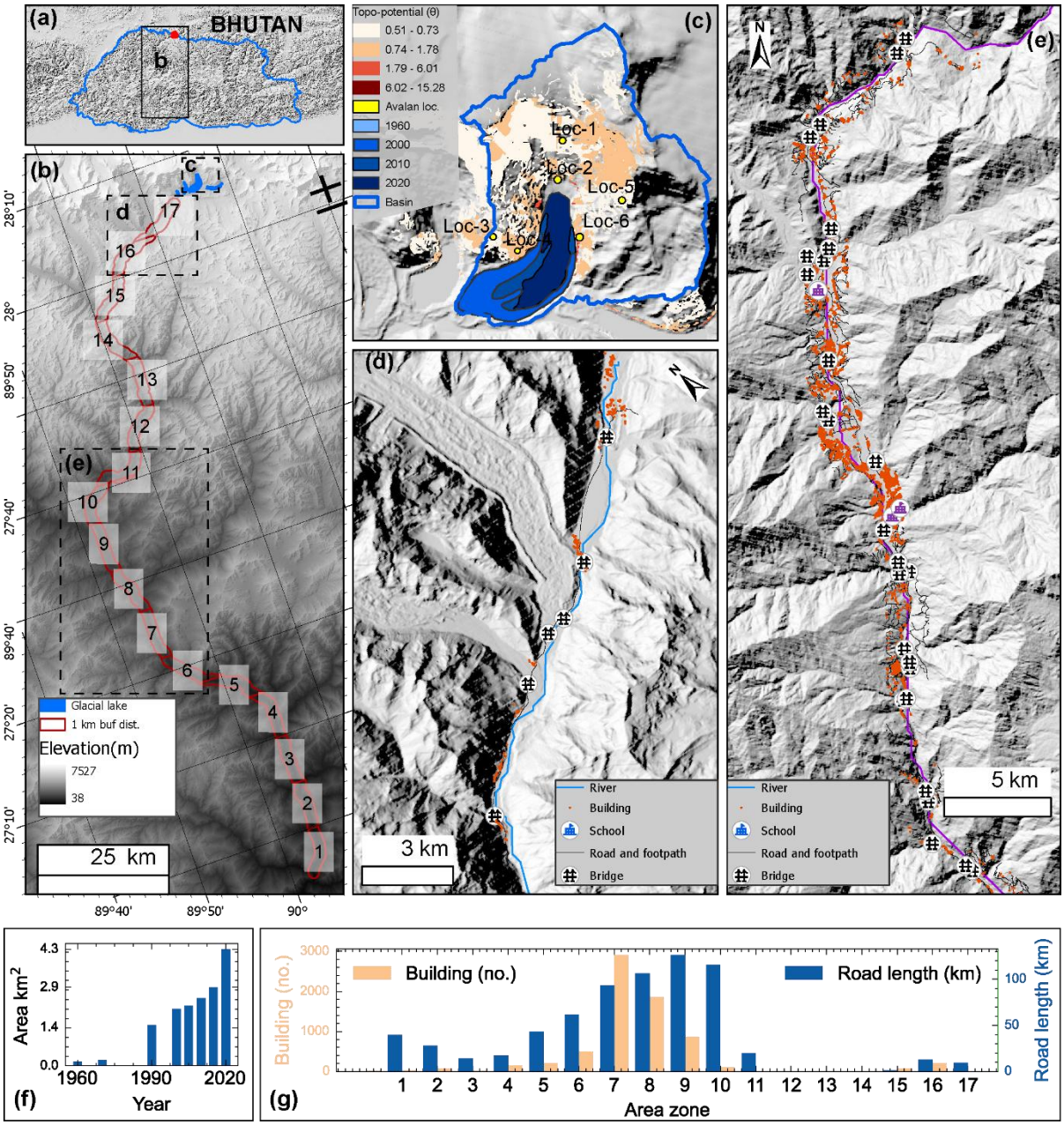

198

199 **Figure 1:** Study area. The map (a) indicates the location of Thorthormi Tsho and its
200 downstream condition in Bhutan. The map (b) shows elevation and the overview of glacial
201 lakes in Lunana and settlements along the Phochu and Punatsangchu basins, downstream of
202 Thorthormi Tsho. The downstream settlement is divided into 17 zones (1-17), each 10 km
203 long. (c) Area of Thorthormi Tsho between 1960 and 2020, and the surrounding slope with
204 topography potential (TPP) for mass movement entering Thorthormi Tsho. ~~(d and e) t~~he
205 downstream settlements in the (d) Lunana and (ed) Punakha and Wangdue Phodrang regions.
206 The bar graphs are (f) the change in the area of Thorthormi Tsho between 1960 and 2020
207 (Rinzin et al., 2023) and (g) the buildings (count) and road (km) within the 1 km on either side

of the river centreline as per the latest OpenStreetMap (as of 30th Mach 2024). Loc-1 to Loc-6 are the locations of origin of mass movement entering the lake considered for this study.

Additionally, the Phochu and Punatsangchu basins, located downstream of Thorthormi Tsho, are the most populated basins in Bhutan. The latest updated (as of 30th March 2024) OpenStreetMap~~,~~ (https://www.openstreetmap.org) although it does not have 100% coverage, shows that there are over 7000 buildings, 50 bridges, 4 schools, 687 km of road and a large area of agricultural land within the 1 km radius of the Phochu and Punatsangchu rivers ~~. 202 buildings are located within the immediate 10 km downstream of Thorthormi Tsho~~ (Fig. 1c,1d,1f). Besides, located downstream are the two biggest hydropower plants (Punatsangchu-1 and Punatsangchu-2) in Bhutan, ~~nearing the commission and~~ poised to become key contributors to the nation's GDP. Also, the Punakha Dzong, which has great ~~great~~ historical and cultural significance to Bhutan is located downstream of Thorthormi Tsho. This high downstream exposure to GLOF hazard further highlights the importance of understanding GLOF characteristics from Thorthormi Tsho for GLOF modelling (Fig. 1).

3 Methods

3. 1 r.avaflow model framework

r.avaflow is a comprehensive GIS-based open-source computational framework for modelling mass movement from one or more release areas over the defined basal topography (Mergili et al., 2017; Mergili and Pudasaini, 2024~~b~~). It can model the entire GLOF process chain starting from the release of avalanches, through the dynamic interaction of the avalanche and lake water, then the overtopping and retrogressive moraine dam erosion, and finally the downstream evolution of the resulting flow (Mergili et al., 2020b; Vilca et al., 2021; Sattar et al., 2023). It can also robustly consider the interactions between the phases as well as erosion and deposition (Mergili et al., 2017). Furthermore, it is equipped with a built-in function for visualization and validation. Because of this capability, r.avaflow has been widely used to model process chains such as GLOF in the high mountains all over the world, mostly to reconstruct past events (Zheng et al., 2021a; Mergili et al., 2020b; Vilca et al., 2021) and to a lesser extent to predict future hazards (Sattar et al., 2023; Allen et al., 2022).

In r.avaflow, the evolution of the flow in space and time is solved by using an enhanced version of the Pudasaini multiphase flow model (Pudasaini and Mergili, 2019; Pudasaini, 2012). The flow is computed through depth-averaged conservation of mass and momentum equations for solid and fluid components. These equations involve six differential equations accounting for solid (D_s) and fluid (D_f) flow depths, solid (M_{sx}) and fluid (M_{fx}) momentum in x direction ($M_{sx} = D_s.v_{sx}$, $M_{fx} = D_f.v_{fx}$), and M_{sy} and M_{fy} in y direction ($M_{sy} = Ds.v_{sy}$, $M_{fy} = D_f .v_{fy}$), where v is the

flow velocity (Mergili et al., 2017). Mohr-Coulomb plasticity is used to compute solid stress while fluid is subjected to solid volume-fraction-gradient-enhanced non-Newtonian viscous stress. r.avaflow also considers other factors like virtual mass force, viscous drag, and buoyancy. These factors collectively facilitate momentum transfer between the solid and fluid phases, enabling simultaneous deformation, separation, and mixing of phases as they propagate across the mountain topography (Pudasaini and Mergili, 2019; Pudasaini and Krautblatter, 2014b; Mergili et al., 2020b; Pudasaini, 2012). To numerically solve these differential equations and propagate flow over time and space, r.avaflow uses a high-resolution total variation diminishing non-oscillatory central differencing (TVD-NOC) scheme, a commonly used numerical scheme to handle the advection of quantities, whilst minimising numerical artefacts like oscillations (Wang et al., 2004). The internal friction angle and basal friction angle, which are crucial factors governing the frictional forces influencing flow rheology, are ~~scaled~~ adjusted based on the ~~with a~~ solid fraction of the flow material (Mergili et al., 2018b; Mergili et al., 2017; Pudasaini and Mergili, 2019). ~~This scaling effectively accounts for the reduced interaction between solid particles and the basal surface within flows rich in fluid (Mergili et al., 2018b; Mergili et al., 2017).~~

r.avaflow has three different models, namely, a single-phase shallow water model with Voellmy friction relation, an enhanced version of the multi-phase-flow of Pudasaini and Mergili (2019) and an equilibrium-of-motion model for ~~the~~ slow-flow process (Mergili and Pudasaini, 2024~~a~~) ~~(Mergili et al., 2017).~~ Here, we chose an enhanced version of the multi-phase-flow model considering an erodible moraine dam and mass movement entering the lake~~rock-ice avalanche~~ as the solid component and lake water as the fluid component. The multi-phase mass flow model can simulate the propagation of three different elements: solid (coarse material including boulders, cobbles and gravel), fine solid (including sand and particles larger than clay and silt), and fluid (including water and very fine particle including clay, silt and colloids), and assign each of them with distinct flow rheology (Pudasaini and Mergili, 2019).

Furthermore, r.avaflow has six specific optional functions including conversion of release height to depth, diffusion control, surface control, entrainment, stopping and dynamic adaption of friction parameters~~-~~. The latest version of r.avaflow has four options to compute erosion and entrainment, (i) calculated by multiplying the entrainment coefficient with flow momentum, (ii) simplified entrainment-deposition numerical model of~~–~~ Pudasaini and Krautblatter (2014a); (Mergili and Pudasaini, 2024~~a~~), (iii) a combination of (i) and (ii), and (iv) acceleration-deceleration entrainment and deposition model. Since models (ii) to (iv) are at the experimental phase, here, we used model (i), where the amount of entrainment is computed dynamically by multiplying with the user-defined entrainment coefficient (CE) with the total

momentum of the flow at the given raster cell and time step (Mergili et al., 2017) (equations 1 and 2).

$$q_{E,s} = C_E|M_s+M_f|\ \alpha_{s,Emax} \quad (1)$$

$$q_{E,f} = C_E|M_s+M_f|\ (1-\alpha_{s,Emax}) \quad (2)$$

Where q_{Es} and q_{Ef} are the entrainment rates of solid and fluid respectively

C_E is user user-defined entrainment coefficient (kg^{-1})

$\alpha_{s,\,Emax}$ is using user-defined solid entertainable material height (m)

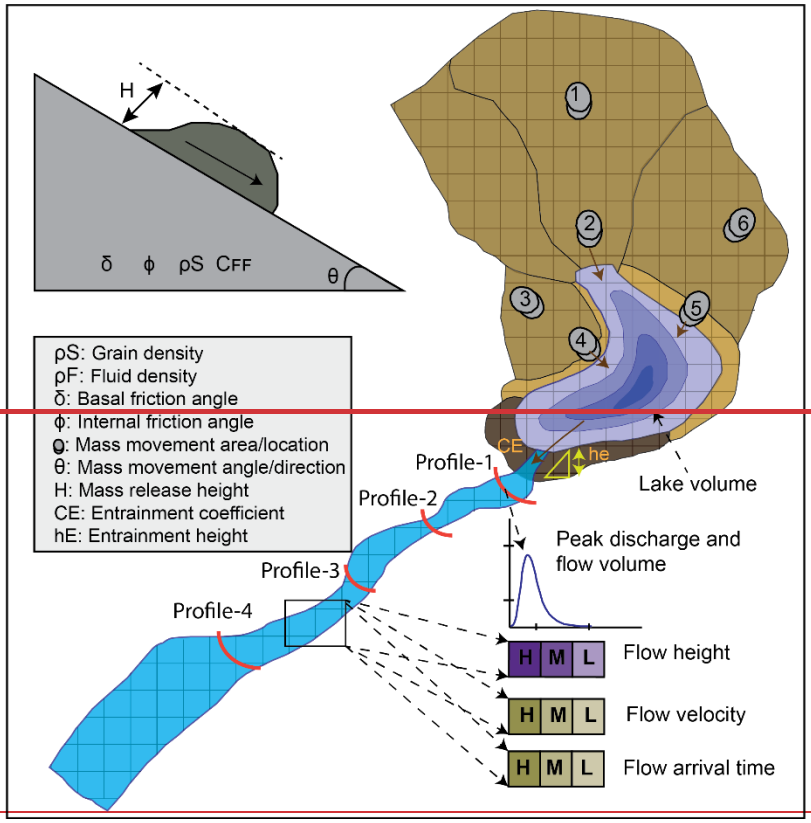

287

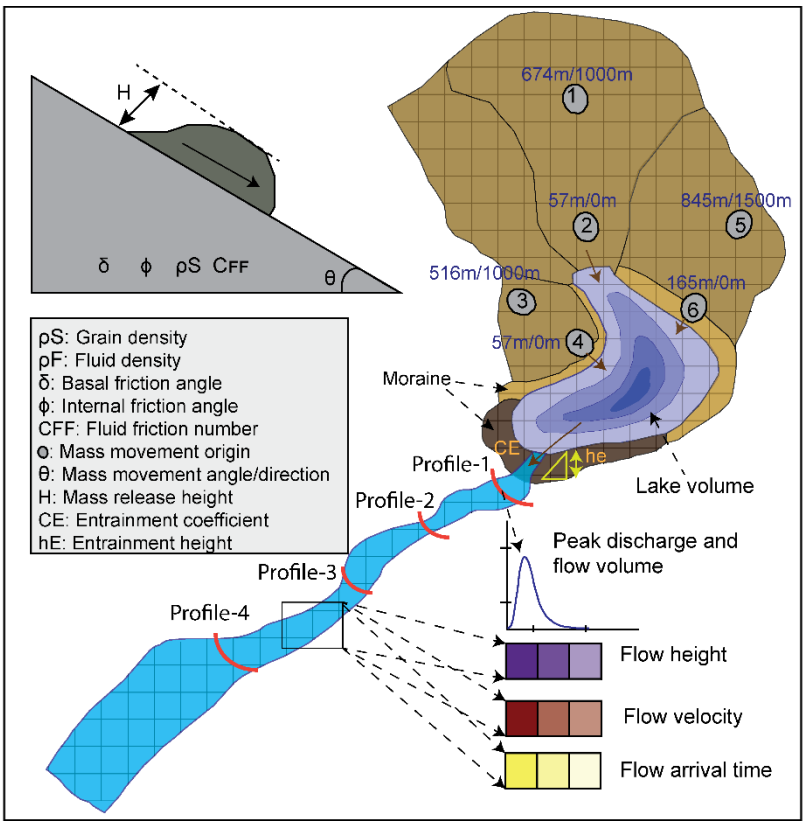

288

289 **Figure 2:** Schematic view of Thorthormi Tsho, surrounding terrain (study area) and input
290 parameters employed for investigating r.avaflow model output sensitivity used in this study. 1-

6 shows the ~~location~~ origin of the mass movement ~~areas into~~ entering the lake (considered for this study) with vertical drop/horizontal distance to the lake shoreline.

We utilized r.avaflow direct, (Mergili and Pudasaini, 2024b, a) ~~(Mergili and Pudasaini, 2024b),~~ a web-based tool (Mergili and Pudasaini, 2024~~b~~), to initially generate the sample model script. We modified ~~it~~ the sample script by inputting parameters relevant to each experimental set-up and wrote a bash shell script for all simulations in each experiment to test various parameter values within our predefined range. We developed one master bash script for each experiment that allowed us to run all experiments in parallel leveraging the Rocket High Performance Computing (HPC) facilities at Newcastle University. All the GLOF simulations were done for Thorthormi Tsho and were run for 1500 seconds when the flow reaches up to ~24 km downstream of the lake depending on values of various parameters defined here. The flow propagation beyond this point and its interaction with the downstream component are beyond the scope of this study.

Table 1~~2~~: Key parameters tested in this study to investigate model output sensitivity. Detailed parameters for r.avaflow modelling are provided in Table S1. The constant value is the common parameter value used across experimental setups.

Parameter	Value range	No. of simulations	Constant value
Topographic data (DEM) ~~and Mesh size~~	High Mountain Asia DEM (HMA-DEM) (8m), AW3D30 (30m), NASADEM (30m), ~~SRTM GL3~~SRTMGL3 (90 m)	~~12~~ 4 (1~~3~~×4)	HMA-DEM
Origin of ~~Avalanche~~ Mmass movement ~~origin location~~	Left (2), Right (2), Headwall (2)	6	Loc-1
~~Avalanche~~ Volume of mass movement ~~volume~~	1 – 10 × 10^6 m^3	10	5 × 10^6 m^3
Grain density of mass movement	1000 – 2700 kg/m^3	10	2700
Lake volume	2 to 3.8 × 10^8 m^3	10	3 × 10^8 m^3
Entrainment coefficient	$10^{-5.85}$ – $10^{-6.95}$ kg^{-1}	10	$10^{-6.35}$
Basal friction angle	10 – 14°	10	10
Internal friction angle	25 – 35°	10	28
Fluid friction number	0.027 – 0.050	10	0.05

3.2 Model inputs parameterisation and experimental setups

In the context of r.avaflow, a parameter is an (often user-defined) variable influencing the physical characteristics of the movement or the numerical behaviour" of the flow. Parameters can be based, e.g., on physics (such as friction angles) or empirical knowledge. Parameters can be represented by global values, by individual values for each raster cell, or by time-dependent values. r.avaflow has a large choice of parameters and initial conditions, such as a DEM representing initial basal topography, the volume of the solid and liquid phase, entrainment and stopping parameters and density and friction parameters (Mergili and Pudasaini, 2024~~b~~) (Table S1). The values specified for these parameters influence crucial aspects of modelled GLOF flow characteristics, including impacted area, travel distance, travel time, and volume of sediment deposited at the various downstream locations (Mergili et al., 2017). In this study we selected a total of nine parameters which are identified as important and commonly modified in the previous studies (e.g. Mergili et al. (2020a)): 1) DEM dataset~~,~~ ~~2) mesh size~~; ~~3)~~ 2) volume of mass movement entering the lake (V_S); 3) the origin of mass movement into the lake; ~~4) volume of mass movement entering the lake;~~ 4) volume of glacial lake (V_L) ~~5~~5) grain density of mass movement entering the lake (ρS); ~~–~~; 6) entrainment coefficient (CE); 7) basal friction angle (δ); 8) internal friction angle (ϕ); 9) fluid frictional number (C_{FF}). To investigate the impact of DEM dataset variation ~~(1) and mesh size variations (2)~~, we modelled GLOF by employing freely available global and regional DEM datasets with differing spatial resolution and vertical accuracy (Table 2). For the origin of the mass movement entering the lake ~~(3),~~ we first computed the topographic potential for ~~slope~~ mass movement into the lake (Allen et al., 2019) (Fig. 1B) and selected six different sites by considering the topographic potential values and ~~direction~~ geometry of the lake (Fig. 2). The ~~volume of mass movement entering lake~~V_S ~~(4)~~ was varied between 1~~0^6 – × 10^6 m^3 and 10 × 10^7~~ ~~10^6~~ m^3. The ~~avalanche~~ ρS ~~grain density (ρS) (5)~~ value range was considered based on assumed combinations of rock and ice ~~avalanche~~ parts in mass movement following the approach used in the earlier studies (Allen et al., 2022; Sattar et al., 2023). For parameters ~~5~~6-9, we gathered various values employed in previous studies (Allen et al., 2022; Mergili et al., 2020a; Mergili et al., 2020b; Vilca et al., 2021) and ~~established the conservative range. In doing so, we~~ computed descriptive statistics and established the median, upper quantile value, and lower quantile for each parameter using these collated values (Fig. ~~–~~S1). We then varied these parameter values between the calculated upper quartile and lower quartile, to give 10 equally spaced values in total. This range of 10 values was utilised in a ~~our~~ total of 10 experiments for ~~the~~ each respective parameter, whilst holding other parameter values constant at the median value. For example, for the ~~internal friction angle (ϕ)~~ experiment, the value of ϕ was varied between the upper and lower quantiles, with 10 increments in total, whilst holding constant the other parameter values (Table 1). An overview of employed parameters and workflow is

shown in Fig. 2 (schematic view) and Table 1, while further details on the parameter range used for each experiment are provided in the following section.

Table 2: Characteristics of DEM datasets employed in this study to investigate the impact of DEM dataset variation on GLOF modelling results.

DEM dataset	Acquisition techniques	Spatial resolution	Vertical accuracy	Coverage	Survey date
AW3D30	Optical stereo images	~30 m	6.84 m (RMSE relative to ICESat in HMA) (Liu et al., 2019)	Global	2006 to 2011
NASADEM	SAR Interferometry	~30 m	5.3 m (RMSE for USA) (Liu et al., 2019)	Global	2000
~~SRTM GL3~~SRTMGL3	SAR Interferometry	~90 m	9.51 m (RMSE relative to ICESat in HMA) (Buckley et al., 2020)	Global	2000
HMA~~- 8m~~ DEM	Optical stereo images	8 m	2-m (depending on the type of sensor) (Shean, 2017a)	High Mountain Asia (HMA)	2002 to 2016

3.2.1 Digital ~~e~~Elevation ~~(1)~~ M~~m~~odel ~~and mesh size (2)~~

Here our goal is to constrain model output uncertainty stemming from the use of freely available global and regional DEM datasets. We performed a series of GLOF simulations using four open-access DEM data of various resolutions, vertical accuracy and elevation derivation methods, namely, High Mountain Asia DEM (HMA-DEM; 8 m) (Shean, 2017b), ALOS Global Digital Surface Model (AW3D30; 30 m) (JAXA~~Jaxa~~, 2021), NASADEM (~30 m) (Nasa-Jpl, 2021), and ~~SRTM GL3~~SRTMGL3 (~90 m) ((Srtm), 2013)~~. Further to investigate the impact of mesh size variation in each DEM dataset, we performed three simulations for each DEM data by changing mesh size to 20 m, 30 m, and 40 m. The GLOF simulations for all other parameter experiments were done using HMA-DEM at 8 m resolution~~ (Table 2). The details about the DEM datasets used here are provided in the supplementary information.

3.2.2 Volume of glacial lake and ~~avalanche~~ mass movement entering the lake ~~(4)~~

r.avaflow has the option to define the initial release volume of different phases involved in the GLOF process chain. Here, we assume the GLOF was initiated by rock-ice mixed mass movement entering ~~into~~ the lake followed by a tsunami wave hitting the moraine damming the lake and causing moraine dam failure. Accordingly, we defined the frontal moraine damming Thorthormi Tsho as phase-1 (rock component with ρ = 2700 kg m~~-~~$^{-3}$), mass movement entering Thorthormi Tsho ~~as~~ as phase-2 (rock-ice component) and Thorthormi Tsho as phase~~-~~-3 (fluid part).

-Field-based bathymetric data is essential for accurately estimating the V_L, which is a fundamental input for the GLOF modelling. However, the ~~due to the location~~remote and harsh environment of glacial lakes in ~~remote mountains and harsh environments, it is~~the mountain regions ~~make~~makes ~~is~~it highly challenging to conduct field-based bathymetric surveys. In the case of Thorthormi Tsho, ~~Conducting a~~ conducting the bathymetric~~y~~ survey is particularly ~~of Thorthormi Tsho is~~difficult ~~highly challenging~~ as the lake is filled with debris and icebergs, which makes it hazardous to conduct survey. In the absence of field-based bathymetry, the area-volume empirical equations are commonly employed by past studies to approximate the V_L. However, these area-volume scales are based on sparse field data and may not represent the actual volume, leading to substantial uncertainties in the volume estimates (Zheng et al., 2021a; Gantayat et al., 2024). In this study, ~~Therefore, we consider~~we calculated the volume of Thorthormi Tsho considering eight area volume empirical equations which are commonly used for computing the volume of moraine dam lakes (Table S2). ~~(Gantayat et al., 2024; Zheng et al., 2021a)~~ Uncertainty in using these empirical equations where evident as the V_L estimate for Thorthormi Tsho ranges between 2.1 × 10^8 m^3 to 3.8 ×10^8 m^3. So, to investigate the impact of this uncertainty on modelled GLOF hydraulics, we modelled 10 scenarios of GLOF by varying V_L from 2.0 ×10^8 m^3 to 3.8 ×10^8 m^3 with increments of 20 ×10^6 m^3. For all other experiments, the ~~d the volume by considering the mean~~median value (2.9~~4~~×10^{8}~~6~~ m^3) of ~~all the volumes~~V_L estimated from ~~a total of eight~~ area-volume scaling equations (Table S2) was used uniformly. ~~This same calculated volume is used as constant fluid volume across all the GLOF simulation experiments we conducted here and was not considered for sensitivity analysis. However,~~ r.avaflow requires spatially varying lake bathymetry to be used as fluid release height rather than the absolute ~~value of lake volume~~V_L. ~~Fortunately,~~ Thorthormi being a recently formed lake, has ice thickness data covering the extent of the lake (Farinotti et al., 2019). Therefore, we computed the bathymetry of Thorthormi Tsho by subtracting ice thickness data from the surface DEM (Linsbauer et al., 2016; Linsbauer et al., 2017). Assuming that the present-day lake has been formed by filling the over-deepening, this ice-thickness-derived bathymetry was adjusted to match the volume ~~we~~ we employed for each ~~calculated from the empirical equation~~modelled GLOF. For example, for the experiment with a V_L of 3 ×10^8 m^3, the ice thickness bathymetry was adjusted to get the same volume (Table S2).

The ~~volume of the avalanche~~ volume of mass movement entering the lake serves as a fundamental parameter for defining various scenarios in the forward modelling of a GLOF (for example, Allen et al. (2022) and Sattar et al. (2023)). However, ~~for the forward modelling purpose,~~ it is difficult to predict how big or small the ~~avalanche~~ mass movement will be. The historical record of V_S is sparse but mostly exceeds 1 × 10^6 m^3 (for example, Zheng et al.

(2021a) and Byers et al. (2018)), although a recent event in Sikkim Himalaya was known to have been caused by a volume of up to 14.7 × 10^6 m^3 (Sattar et al., 2025). Additionally, earlier studies in Nepal based on topographic potential and assumed three depths based on avalanches in Russia and the Swiss Alps (10m, 30m and 50 m) (Rounce et al., 2016) has estimated the volume between 2.7 × 10^6 to 6.7 × 10^6 m^3 (Sattar et al., 2021a). Here we selected the most likely zone of mass movement entering lakes based on the topographic potential of the slope surrounding the lake. However, accurately constraining the V_S remains highly challenging and subject to considerable uncertainty. Considering these uncertainties, to test the effect of mass movement of various volumes, we conducted a series of 10 experiments considering volumes V_S ranging from 1×10^6 to 10×10^6 m^3. For the other experiments, we used a uniform V_S of 5 × 10^6 m^3 (Table 1).

3.2.3 Origin of mass movement into the lake

To account for uncertainties involved in the in the exact origin of mass movement into entering the lake, we identified a total of six mass movement areas, each characterised by different directions and , distances, and angles to the lake (Fig. 1 and Fig. 2). To do this, we first computed topographic potential for mass movement (ice/rock avalanche and landslide) movement into the lake based on slope and run-out trajectory criteria (Allen et al., 2019). Based on this first-order estimate, we identified the six potential avalanche mass movement source areasorigin each with unique direction, height, and distance relative to the lake (Fig 2): Loc-1 (slope at ~1 km~900 m away from the headwall, aligned along the longitudinal axis), Loc-2 (headwall about 100 m away from the lake along the longitudinal axis), Loc-3 (slope at the 1 k~900 m from right moraine dam), Loc-4 (right moraine dam), Loc-5 (slope at ~900 1.5 km from left moraine dam), Loc-6 (left moraine dam) (Fig. 1 and Fig. 2). We then ran one scenario for of GLOF from each of these locations (total = 6) keeping all input variables constant for each model run. For the rest of the experiments, we used a mass movement scenario from loc-1.each potential avalanche input location we identified.

3.2.4 Grain density of mass movement entering the lake (5)

Our goal here is to assess the impact of the grain density of the mass movement ρS entering the lake, which serves as a proxy for the ice-to-rock ratio. Accordingly, we consistently set the grain density of phase-1 (moraine) at 2700 kg m^{-3} across all the experiments, whilst the fluid density of phase-3 was also held constant at 1000 kg m^{-3}. In the earlier studies, ρS the grain density of mass movement has entering the lake has been used as a proxy of the portion of an ice-rock component of mass movement into the lake, which is highly uncertain (Vilca et al., 2021; Allen et al., 2022). The phase separation of rock and ice components of the mass

movement with different densities is not well established in r.avaflow (Vilca et al., 2021). Therefore, in this study, following Sattar et al. (2023), a portion of snow and ice in the ~~avalanche~~ mass movement is considered fluid by adjusting the ρS ~~material density~~ of the phase-2 represented by the ~~avalanche~~ mass (Table S3). In our experiment set-up, this is executed by varying the ρS ~~density~~ value between 2700 kg m^{-3} (representing 100% rock) to 1000 kg m^{-3} (representing 100% ~~water~~ice) (Table 1).

3.2.5 Entrainment coefficient ~~(6)~~

Material entrainment due to bed erosion can make the flow more concentrated and thus increase the volume, resulting in spatial and temporal variation of flow. In the r.avaflow model, the user must define entrainment height in the form of a raster covering the entire model domain, which can be either identified using remote sensing imagery or fieldwork (Mergili and Pudasaini, 2024~~b~~). However, accurately measuring the depth and spatial extent of these erodible materials covering the entire model domain is highly challenging, even with field surveys, and remains infeasible using remote sensing techniques alone. In this study, we focused on the frontal moraine, as it is measurable using remote sensing data. The extent of the moraine was mapped using high-resolution Google Earth imagery, while its height was determined using the HMA-DEM~~However, here, we considered frontal moraine damming the lake as the only entrainment height~~ (Fig. 1). The amount of entrainment itself is dependent on the user-defined ~~entrainment coefficient (~~C_E~~)~~. In r.avaflow the logarithm with base 10 of the C_E must be entered (Mergili et al., 2018a; Mergili et al., 2017). Here, we modelled 10 scenarios of GLOF by varying C_E between $10^{-6.95}$ to $10^{-5.85}$ kg^{-1} (Table 1).

3.2.6 Frictional parameters ~~(7–9)~~

The internal friction angle (ϕ), basal friction angle (δ) and fluid friction number (C_{FF}) mechanically control the basal shear stress, internal deformation, anisotropy of the stresses, and hydraulic pressure gradient of the solid constituents (Pudasaini and Krautblatter, 2014b), which are essential attributes influencing flow runout distance and time. Within the r.avaflow model set-up, a user can either use spatially varying values for these frictional parameters using a raster map or one absolute value (Mergili and Pudasaini, 2024~~b~~; Mergili et al., 2017). In this study, we computed 10 experiments for each of these frictional parameters. Specifically, by varying ~~the~~ ϕ~~ϕ~~ between 25° to 35°, δ between 10° and 14° and C_{FF} between 0.027 to 0.050 (Table 1).

3.3 Sensitivity Analysis

Here we use sensitivity analysis, to determine how variations in the initial values for key input parameters impact the modelled ~~output~~GLOF hydraulics~~s~~ (Saltelli et al., 2004). Thus, our goal is not to determine the 'correct' value for each parameter but to determine the r.avaflow input parameter(s) that cause the most variation in the model output. To constrain this variability, we mainly focused on examining the peak discharge, total discharge, and flow arrival time as the output metrics. The flow for all the experiments was measured from the profile immediately beneath the moraine dam (profile-1 in Fig. 2). We calculated the peak and total discharge based on the flow data obtained from the same profiles (Fig. S2). The flow arrival time was considered as the average value across the time recorded from the profiles located 3 km, 6 km and 9 km downstream of the Thorthormi Tsho (profile-2, 3, 4 in Fig. 2). ~~All input parameters were standardized within a percentile range of 0 to 100 for comparative analysis of their effects on the resultant outputs.~~ For the scalable parameters, we also computed simple linear regression considering input parameters as the independent variable and model output as the dependent variable. To ascertain the sensitivity of the three model output metrics defined earlier to variations in value across all parameters, we computed the coefficient of variation (CV) for individual parameters and subsequently ranked them based on this metric. The CV is a statistical measurement of the dispersion of data points around the mean, regardless of the units used to measure it. CV is deemed suitable here since the r.avaflow output variability is caused by input parameters that are measured in different units. To calculate CV, we took the standard deviation of the output value range of a particular experiment (e.g. peak discharge) and divided it by the mean of the same output range (Abdi, 2010). We multiplied each CV value by 100 to express them in percentage form.

4 Results

4.1 Effect of DEM dataset

When the GLOF wa~~i~~s modelled employing freely available global and regional DEM datasets (HMA-DEM, AW3D30, NASADEM, ~~SRTM-GL3~~SRTMGL3), our results showed a variation of peak and total discharge of GLOF from the Thorthormi Tsho by almost 100% and 400%, respectively (Fig. 3). Specifically, HMA-DEM consistently produced the lowest GLOF magnitude, while ~~SRTM-GL3~~SRTMGL3 consistently produced the highest. ~~The peak flow fluctuates between 10-115% and the total discharge between 55-400% (Fig. 3).~~ Although NASADEM and AW3D30 have a similar spatial resolution, notable differences (65%) in peak discharge and other hydraulic properties emerged between simulations done using these datasets (Fig. 3a~~b and 3c~~).

We observed a significant fluctuation in the mean ~~flow height~~flow depth (82%) and velocity (~~65~~43%) along the flow path resulting from the change in DEM datasets (Table~~Fig~~. 3). For instance, the mean ~~flow height~~flow depth along the river centreline ranged from 39 m (HMA-DEM) to 54 m (~~SRTM GL3~~SRTMGL3) (Table 3) and the flow reach distance increased from 15.5 km (HMA-DEM) to 24.2 km (~~SRTM GL3~~SRTMGL3). Once again, NASADEM and AW3D30 yielded significantly different maximum ~~flow height~~flow depths (8.5%) and reach distances (72%) (Fig. 3b ~~an~~)~~d 3c)~~. ~~The use of various sources of DEM datasets led to variations in~~The ~~total~~ flow arrival time varied ~~by~~ by around ~~16~~59%. Flows derived from SRTM data always arrived earlier, while those using HMA-DEM were consistently ~~showed the latest arrival times~~most delayed (Fig. 3c) ~~(Table 3)~~. ~~For example, at 5 km downstream, SRTM GL3 showed the earliest arrival at 3.46 min while HMA-DEM resulted in the latest arrival at 4.37.~~ There was also a ~~The portion of the~~similar variation in the solid ~~component~~ concentration of the flow ~~did not exhibit significant fluctuations~~ in response to changes in input DEM datasets (Fig. 3b).

~~4.2 Effect of mesh size variations~~

~~When mesh size was increased from 20 m to 30 m and 40 m across all the DEM datasets, we noted a substantial increase in peak and total discharge, resulting in significant increase in flow characteristics like flow depth (Fig. 3). For instance, in the case of the experiment with HMA-DEM, the peak discharges increased to 20% and 38%, respectively (Fig. 3). However, the mean flow velocity increased only by 6% when the mesh size was increased from 20 to 40 m (Table 3). Likewise, there was no significant difference in the flow reach distance emerging from changing mesh size (Fig. 3). For instance, flow with all three mesh sizes for HMA-DEM resulted in to flow reach distance of about 15 km (Fig. 3a). Mesh size variation resulted in arrival flow time variation of about 20%, with 40 m leading to earliest arrival and 20~~

~~m the latest (Table 3).~~

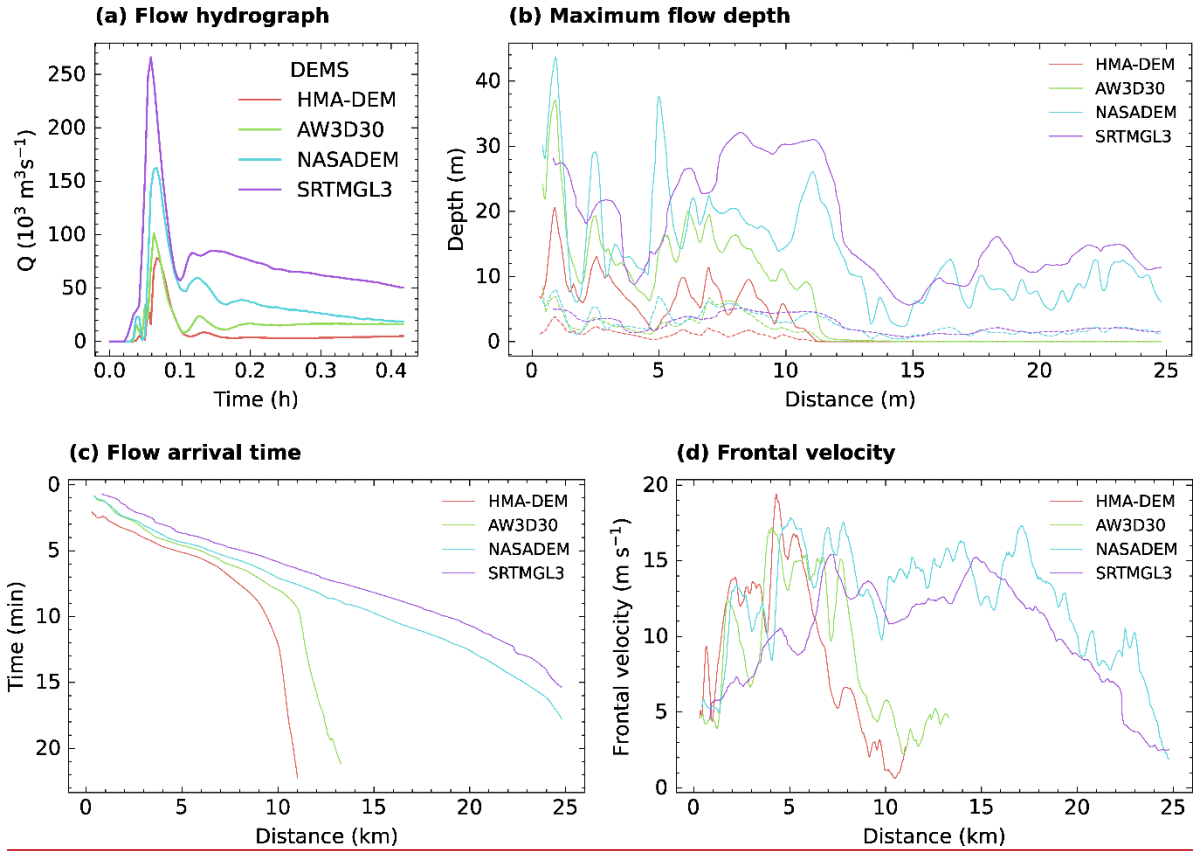

Figure 3: The line graph (a) showing hydrographs ~~(right panels) measured at just below the moraine,~~ (b) maximum ~~flow height~~flow depth (for total and debris part), (~~c~~b) flow arrival time and (d) ~~frontal~~ flow velocity profiles along the river centerline ~~left~~ generated by conducting a sequence of r.avaflow simulations, employing different types of DEM datasets. The solid and dashed lines (in panel a) show the maximum flow depth and~~the~~ debris part of the flow. The profiles are plotted as rolling averages every 100 m. ~~.change the axis~~

Table 3. Percentage change in flow velocity, depth and arrival time resulting from variation in values of different input parameters we employed in this study. The total percentage (%) change represents the output variation between the maximum and minimum values used in the experiment. The average percentage (%) change is calculated as the mean change across all incremental steps employed in setting up the experiment. The arrival time average of the record from three locations, Profile-2, -3, and -4) (Fig. 2). Flow velocity and depth are mean values taken from the river centreline. The negative (-) value indicates that increasing input parameters decreases output parameters. The ~~detail~~ detailed flow pattern along the river centreline is provided in Fig. S3, Fig. S4, ~~and~~ Fig. S5 and Fig. S6.

N~~SL n~~o.	Parameter	Velocity (% change)	~~Depth~~ (Depth (% change)	Time (% change)

		Average	Total	Average	Total	Average	Total
1	DEM dataset	16.25	6543	20.5	82	204	5916
2	Mesh Resolution	2	6	3	9	4	12
23	Volume of mass movement entering lake	9.2	92	92.3	923	-14.3	-143
34	Density of mass movement entering the lake movement entering lake	0.2	2	3.1	31	-0.6	-6
45	OLocation of origin of mass movement entering the lake movement entering lake	3.710.8	3765	8.2	82	3.38	208
56	Volume of glacial lakeEntrainment coefficient	0.11	110	0.14.9	149	-43	-93
6	Entrainment coefficient	-1	-10	-4.9	49	3	3
7	Basal friction angle	-2.3	-23	-4.2	42	6.8	68
8	Internal friction angle	-0.1	-1	-3.8	38	0	0
9	Fluid friction number	-5.5	-55	-7	70	0.8	8

4.2 Effect of origin of mass movement entering the lake

We modelled mass movement with a volume of 5 × 10^6 m^3 entering the lake from the surrounding slopes at various locations identified in section 3.2.3. Our study found that the GLOF process chain initiated by mass movements from various locations locations (Loc-1 to Loc-66) results in a significant fluctuation in the GLOF output (Fig. 4). The peak discharge varied by approximately 200%, and the total discharge by 55% (Fig. 4). Likewise, the mean flow heightflow depth, and velocity and arrival time also fluctuated by 65%, and 82%, 20%, respectively (Table 3). By comparison, the flow resulting from the GLOF initiated by mass entering from the Loc-1 (Fig. 4a) (900 m1 km from the headwall) and Loc-5 (~1.5 km above the left moraine) (Fig. 4e) produced the highest magnitude GLOF and that from the loc-4 (right lateral moraine) (Fig. 4d) was the lowest. For example, the highest peak (180 × 10^3 m^3) and total discharge (11 ×10^6 m^3) occurred from Loc-1, while the lowest peak (6,0000 × 10^3 m^3) and total discharge (7 × 10^6 m^3) were from Loc-4 (right lateral moraine) (Fig. 4a and 4d). The longest flow reach distance (25 km) was produced by Lloc-1 and Lloc-5, while the shortest was from minimum from Lloc-3 (10 km) (Fig. 4c)). Arrival times vary approximately by 20%, where the flow from Loc-5 arrives earlier while Loc-1 arrives at the latest (Table 3 and Fig. 4). Solid volumetric portion did not exhibit significant fluctuation, with concentration ranging from 4% (Loc-4) to 5% (Loc-2) (Fig. S3Fig. 4).

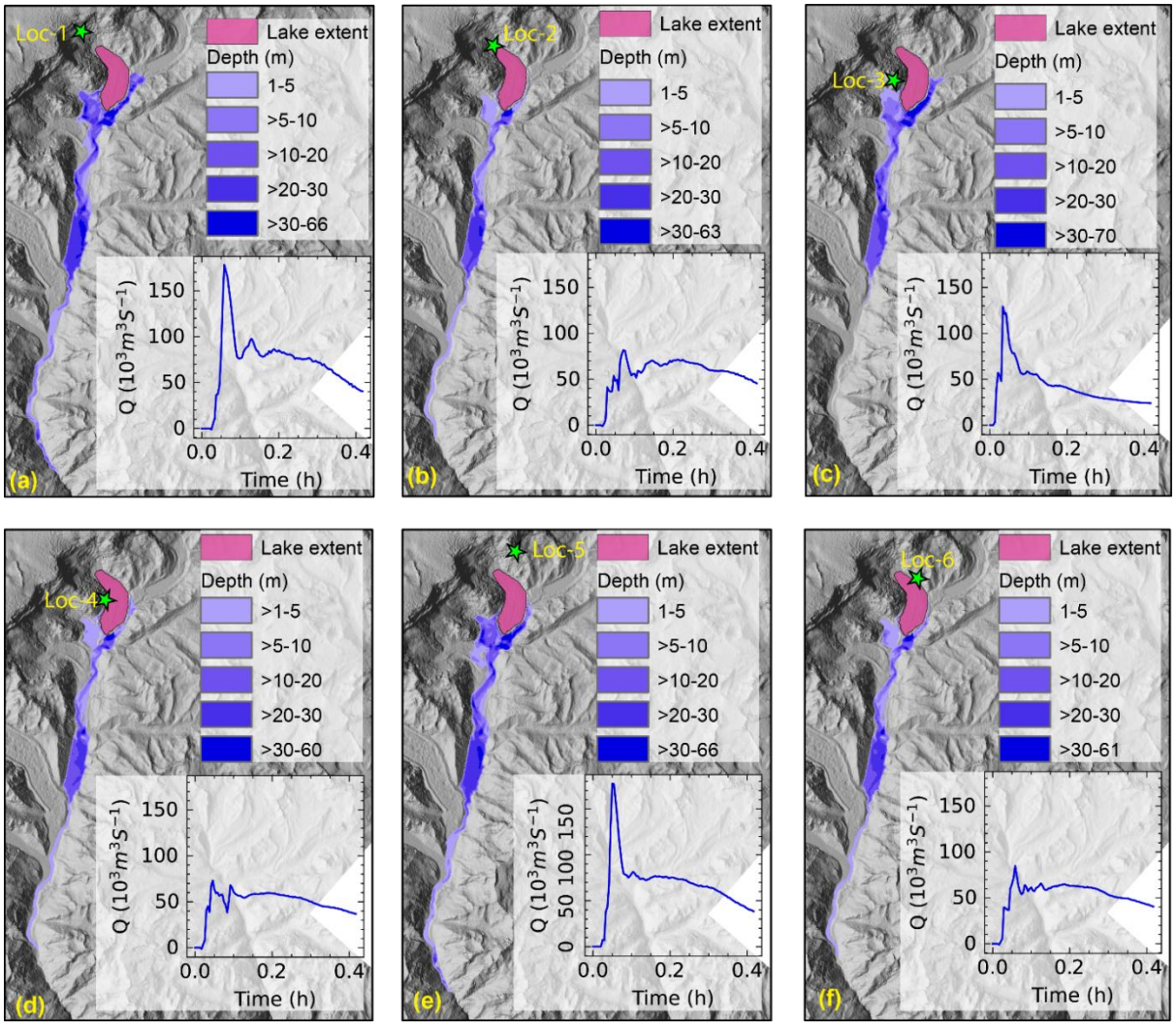

Figure 4: Flow rate and depth resulting from mass movement into the lake from different locations: loc-1 (a) to loc-6 (f).

4.3 Effect ~~of volume and grain density~~ of volume and grain density of mass movement entering the lake

To separate the effect of variation in volume ~~volume~~ V_S and grain density ~~density (~~ρS~~) of mass movement entering the lake,~~ of mass movement entering the lake, we simulated all 10 scenarios of the GLOF event for each volume and density variation using the mass movement initiated from loc-1. Here we observed that only ~~volume~~ V_S variation ~~in mass movement~~ leads to a very large variation in the resulting peak (1160%) (Fig. 5a) and total ~~flow~~ discharge (2500%) (Fig. 6a). Subsequently, this resulted in maximum variation in flow characteristics such as mean ~~flow height~~flow depth (923%) and flow arrival time (143~~50~~%) (Table 3, Fig. S3–S6~~, Fig S5~~). Conversely, the ρS variation showed the least impact on both peak (5%) and total discharge (24%) (Fig. 5b, ~~Fig.~~ 6b, and ~~Fig.~~ 7b) and subsequent characteristics such as ~~flow height~~flow depth (31%) and velocity (2%) (Table 3 and Fig. S3–S6~~5~~). Both ~~volume~~ V_S and ρS

~~density~~ variation did not result in significant fluctuation in the solid-volumetric concentration of the flow (Fig. S3).

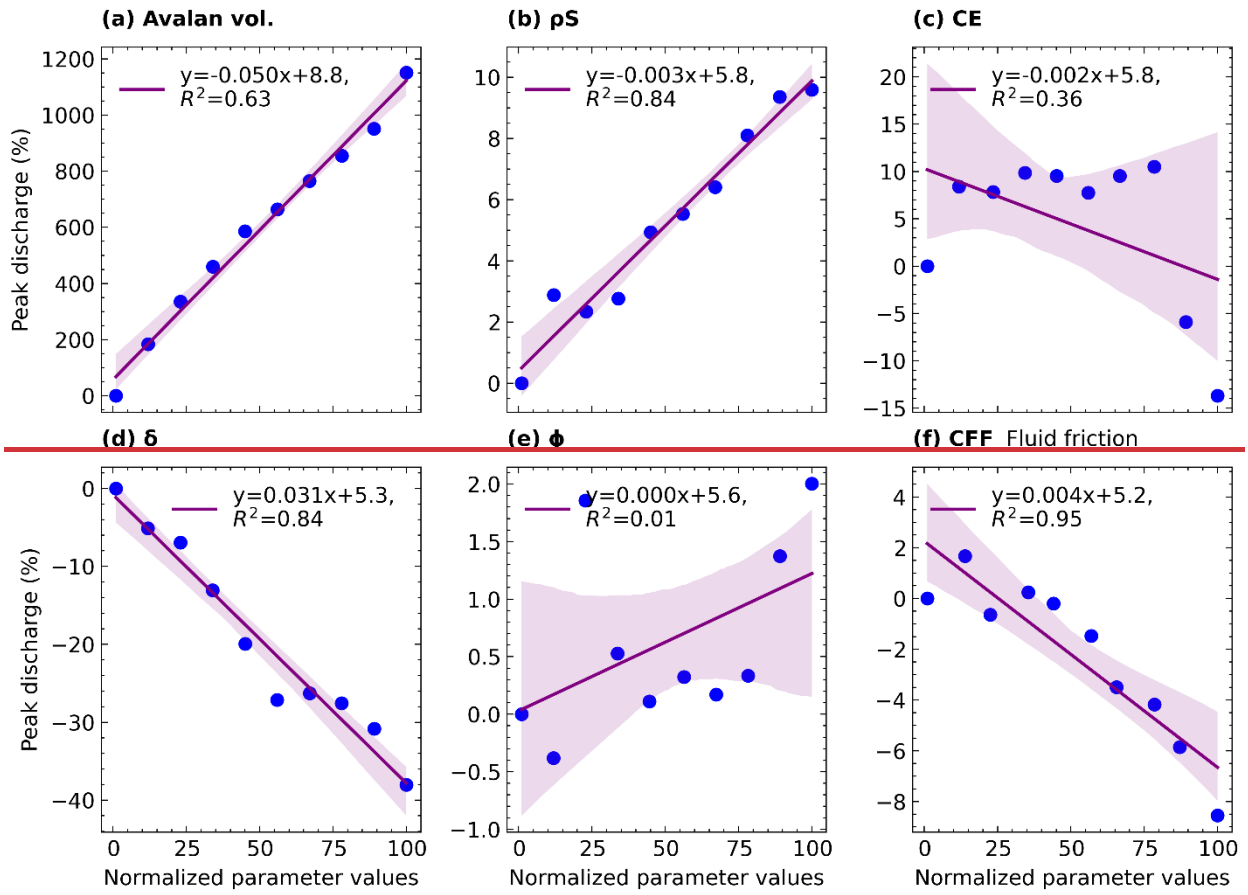
(a) Avalan vol.
(b) ρS
(c) CE
(d) δ
(e) ϕ
(f) CFF Fluid friction
y=-0.050x+8.8, R^2=0.63
y=-0.003x+5.8, R^2=0.84
y=-0.002x+5.8, R^2=0.36
y=0.031x+5.3, R^2=0.84
y=0.000x+5.6, R^2=0.01
y=0.004x+5.2, R^2=0.95
Peak discharge (%)
Normalized parameter values

578

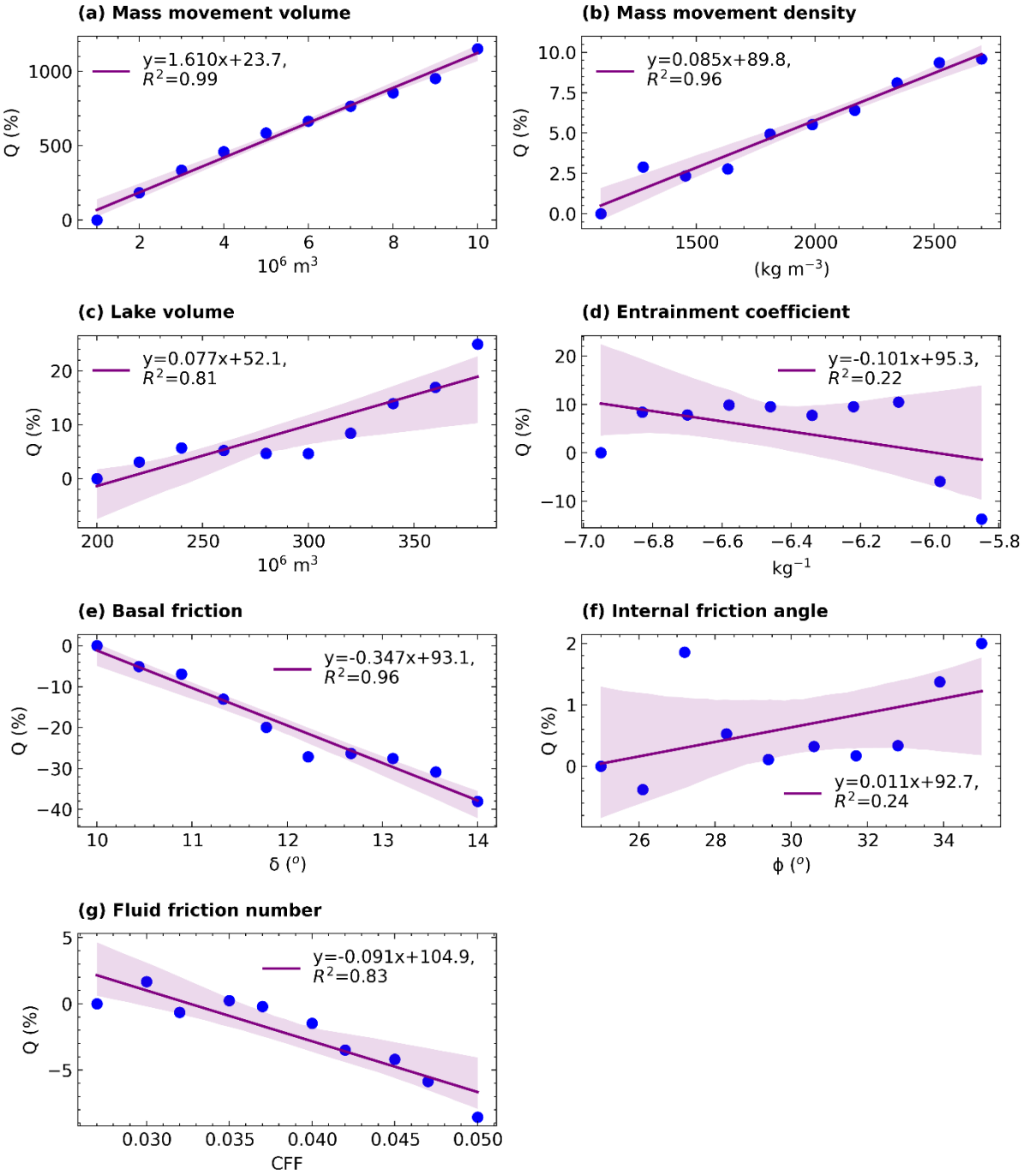

Figure 5: Linear regression between input parameter value variation and percentage change in resulting peak discharge~~. All input parameter values are normalized between 0 to 100~~. The linear regression is computed only for the scalable parameters (a) volume of mass movement into the lake ~~(a)~~, (b) mass movement~~grain~~ density ~~(b),~~ (c) volume of glacial lake (d) entrainment coefficient ~~(c)~~, (e) basal friction angle ~~(d)~~, (f) internal friction angle ~~(e)~~ and (g) fluid friction number ~~(f)~~. The shaded envelope around the line shows a 95% confidence interval.

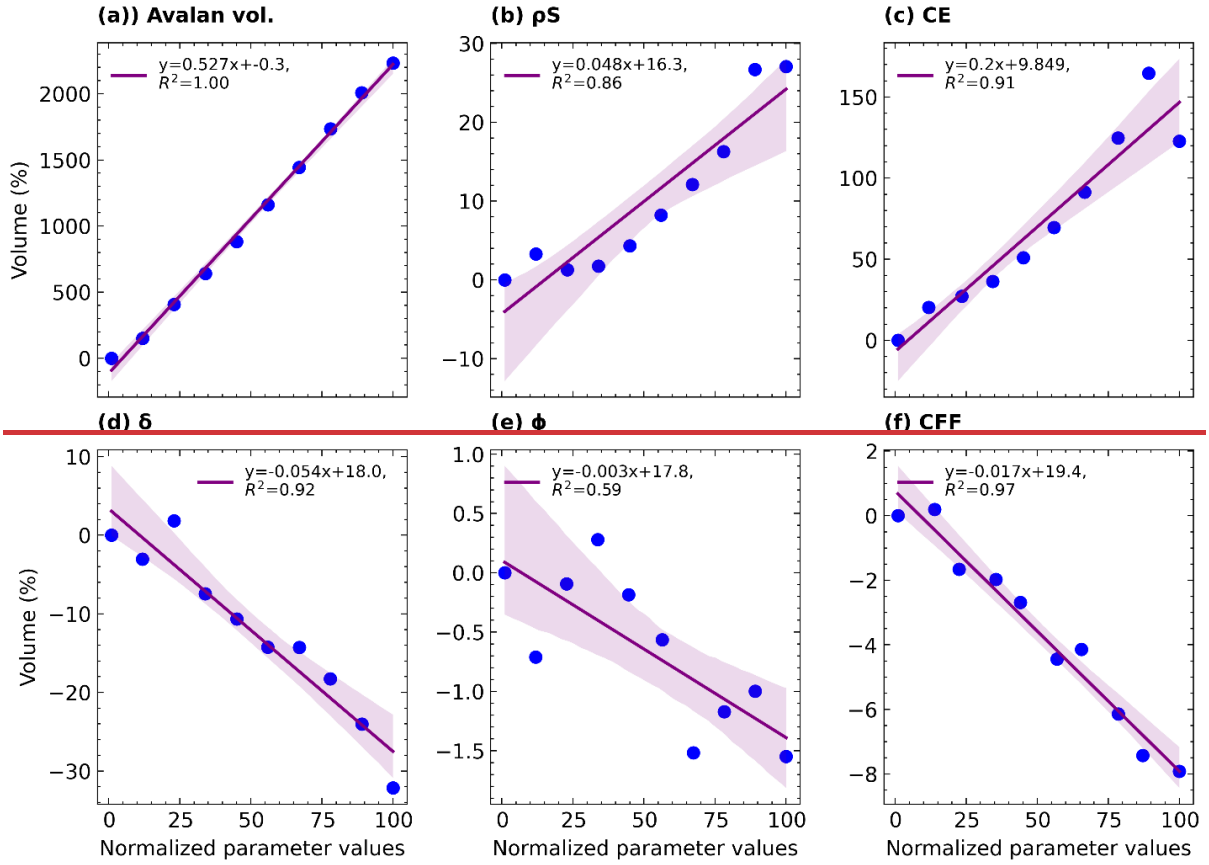
(a)) Avalan vol.
y=0.527x+-0.3,
R^2=1.00
Volume (%)
(b) ρS
y=0.048x+16.3,
R^2=0.86
(c) CE
y=0.2x+9.849,
R^2=0.91
(d) δ
y=-0.054x+18.0,
R^2=0.92
Volume (%)
Normalized parameter values
(e) ϕ
y=-0.003x+17.8,
R^2=0.59
Normalized parameter values
(f) CFF
y=-0.017x+19.4,
R^2=0.97
Normalized parameter values

588

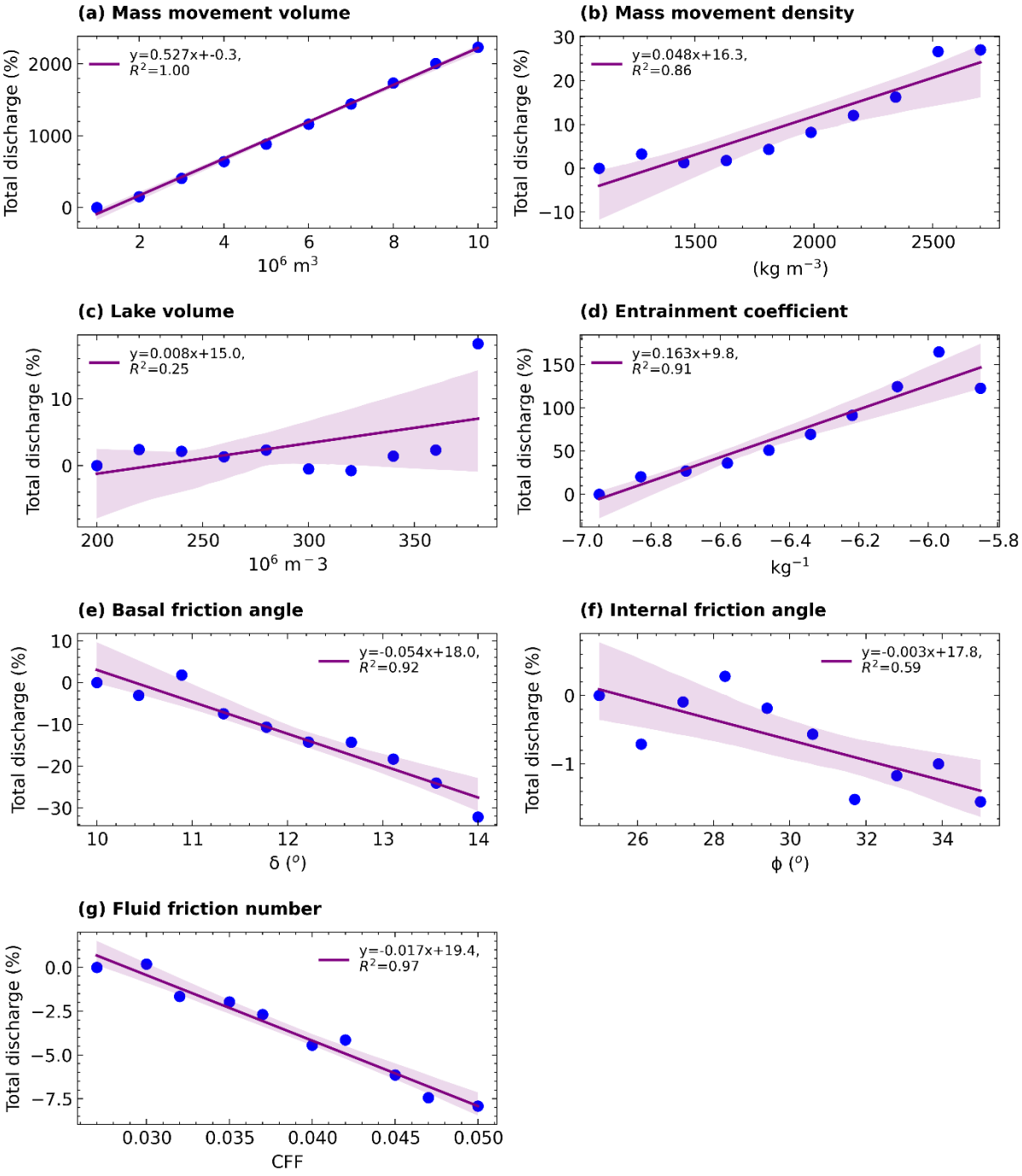

Figure 6: Linear regression between input parameter value variation and resulting total discharge. ~~All input parameter values are normalized between 0 to 100.~~ The linear regression is computed only for the scalable parameters (a) volume of mass movement into the lake, (b) mass movement density (c) volume of the lake (d) entrainment coefficient, (e) basal friction angle, (f) internal friction angle and (g) fluid friction number. The shaded envelope around the line shows a 95% confidence interval.

~~The linear regression is computed only for the volume of mass movement into the lake (a), grain density (b), entrainment coefficient (c), basal friction angle (d), internal friction angle (e) and fluid friction number (f)~~.

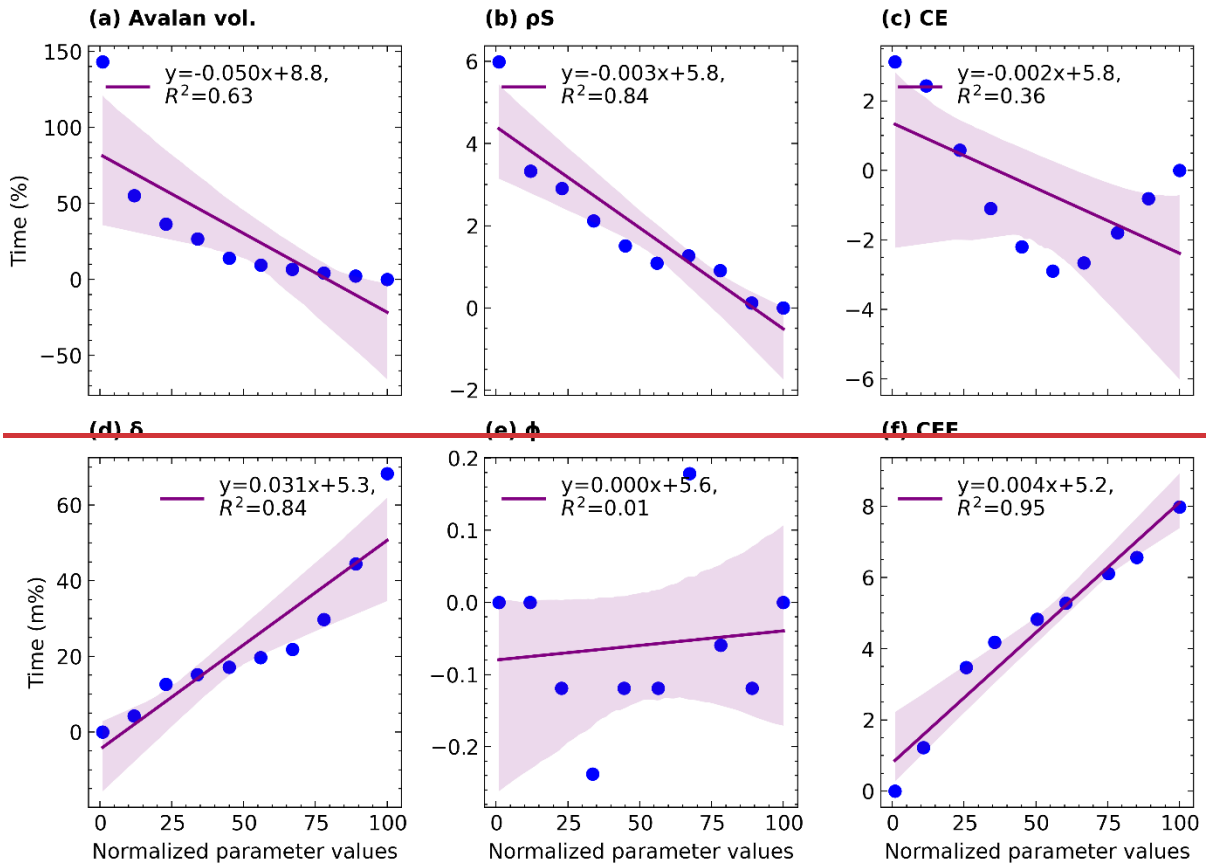
(a) Avalan vol.
y=-0.050x+8.8,
R^2=0.63
Time (%)
(b) ρS
y=-0.003x+5.8,
R^2=0.84
(c) CE
y=-0.002x+5.8,
R^2=0.36
(d) δ
y=0.031x+5.3,
R^2=0.84
Time (m%)
Normalized parameter values
(e) ϕ
y=0.000x+5.6,
R^2=0.01
Normalized parameter values
(f) CEE
y=0.004x+5.2,
R^2=0.95
Normalized parameter values

599

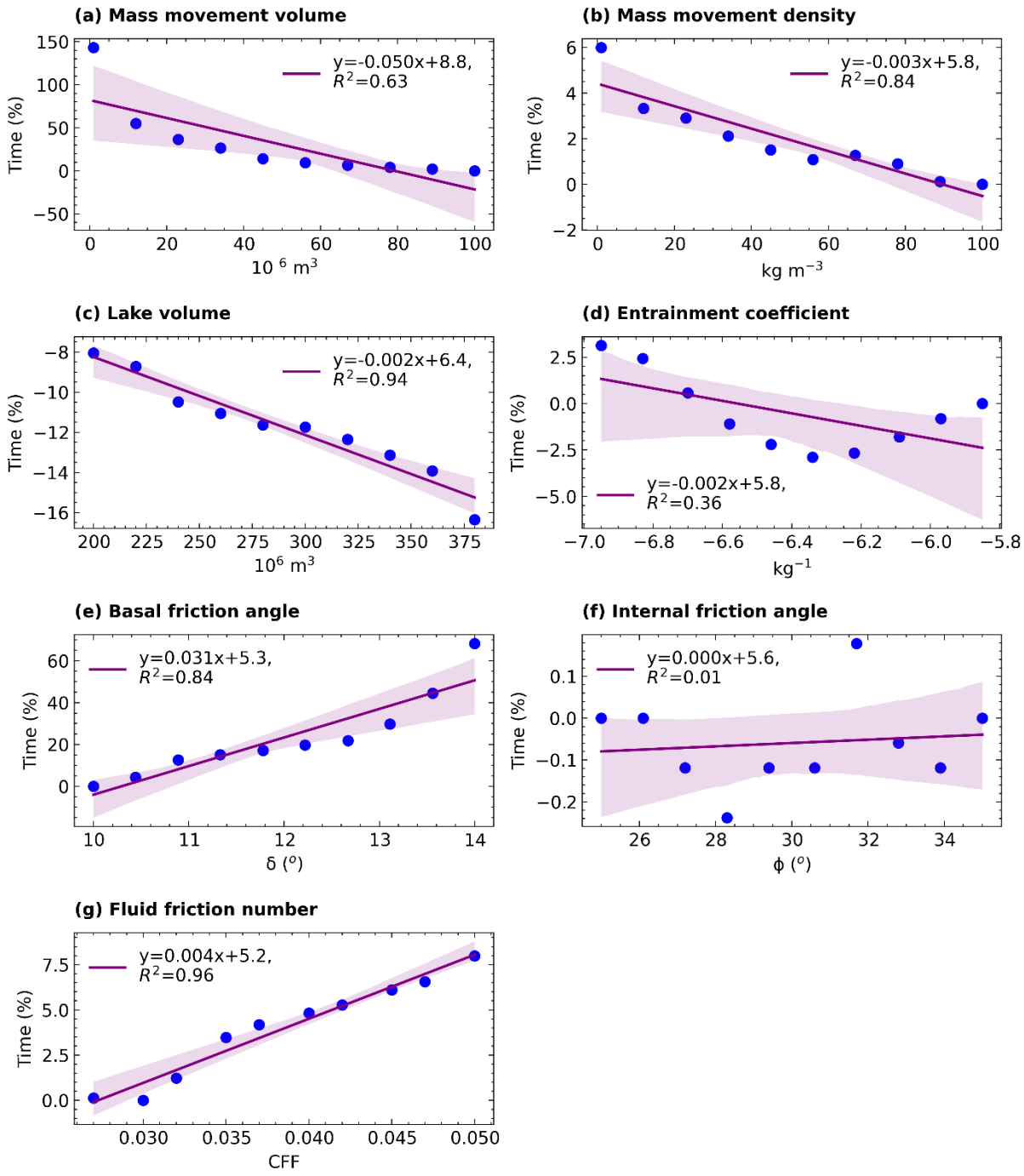

Figure 7: Linear regression between input parameter value variation and flow arrival time. The linear regression is computed only for the scalable parameters (a) volume of mass movement into the lake, (b) mass movement density (c) volume of the lake (d) entrainment coefficient, (e) basal friction angle, (f) internal friction angle and (g) fluid friction number. The shaded envelope around the line shows a 95% confidence interval.

~~**All input parameter values are normalized between 0 to 100. The linear regression is computed only for the volume of mass movement into the lake (a), grain density (b),**~~

~~entrainment coefficient (c), basal friction angle (d), internal friction angle (e) and fluid friction number (f)~~4.4 Lake volume

Variation in volume of the glacial lake (V_L) from 2 to 3.8 × 10^8, results in total peak discharge variations of 25% with an average of 8.7% (Fig. 5c). Likewise, the total discharge varied by 18% with a mean variation of 3% (Fig. 6c). However, the resulting flow characteristics including flow depth, velocity (Table 3) and arrival time (Fig. 7c) all showed minimal fluctuation, as the total percentage change was well below 10% (Table 3).

4.~~5~~5 Effect of entrainment coefficient

Variations in the entrainment coefficient (~~entrainment coefficient~~C_E) substantially impact the resulting GLOF output, causing fluctuations in ~~in peak~~ total discharge ~~and volume~~ by ~~13% and~~ 123%, ~~respectively~~ although its impact on peak discharge was minimal (13%) (Fig. 5d~~c~~ and 6d~~c~~). ~~–~~These changes also affect the flow characteristics including mean depth (49%) and reach distance (20%) (Table 3) but had minimal effect on arrival time (3%) (Fig. 7d~~c~~). Interestingly, CE variation exhibited threshold effect on peak discharge, total discharge and flow arrival time. The total discharge increases linearly with increasing C_E up to $10^{-5.97}$ kg^{-1} but decreases after this. On the other hand, peak discharge increased when C_E increased from $10^{-6.95}$ to $10^{-6.83}$ kg^{-1}, remained constant between $10^{-6.83}$ kg^{-1} and $10^{-6.09}$ kg^{-1} and decreased from there on. The arrival time decreased when the C_E value was increased from $10^{-6.46}$ kg^{-1} to $10^{-6.46}$ kg^{-1} but increased upon further increase of CE value to $10^{-5.85}$ kg^{-1}. ~~Most~~ Also~~notably~~, unlike other parameters, entrainment variation ~~also~~ affected the solid concentration of the flow (Fig. S3). An increase in the entrainment coefficient from $10^{-6.95}$ to $10^{-5.85}$ kg^{-1} led to a 30% increase in the mean solid volumetric concentration of the flow.

4.~~6~~6 Effect of frictional parameters

Among the frictional parameters, basal friction angle (~~the variation in basal friction angle (~~δ~~)~~) resulted in a significant fluctuation in GLOF magnitude (Fig. 5e, 6e, 7e) and ~~resulting~~ subsequent flow characteristics (Fig. S3–S6) ~~(Fig. 5d, 6d and 7d)~~. While the variation of fluid friction number (~~fluid friction angle~~C_{FF}) had minimal impact on the resulting peak and total flow (Fig. 5~~e~~g, 6g~~e~~), it notably altered other flow characteristics, such as flow velocity (55%) and depth (70%) (Table 3). The ~~δ angle~~ increase of δ from 10 to 14° resulted in a peak and total discharge decrease of 36% (Fig. 5d) and 32% (Fig. 6d), respectively. ~~—~~ Likewise, the flow velocity decreased by 23% resulting ~~into~~ in a delay in flow arrival by 6~~1~~8% (Table 3). Conversely, the peak flow decreased by 2% only in response to an increase in the internal

friction angle (~~internal frictional ϕ) angle~~ from 25-35° (Fig. 5f). The variation in all frictional parameter values did not result in a significant change in the solid volumetric concentration of the flow (Fig. S54).

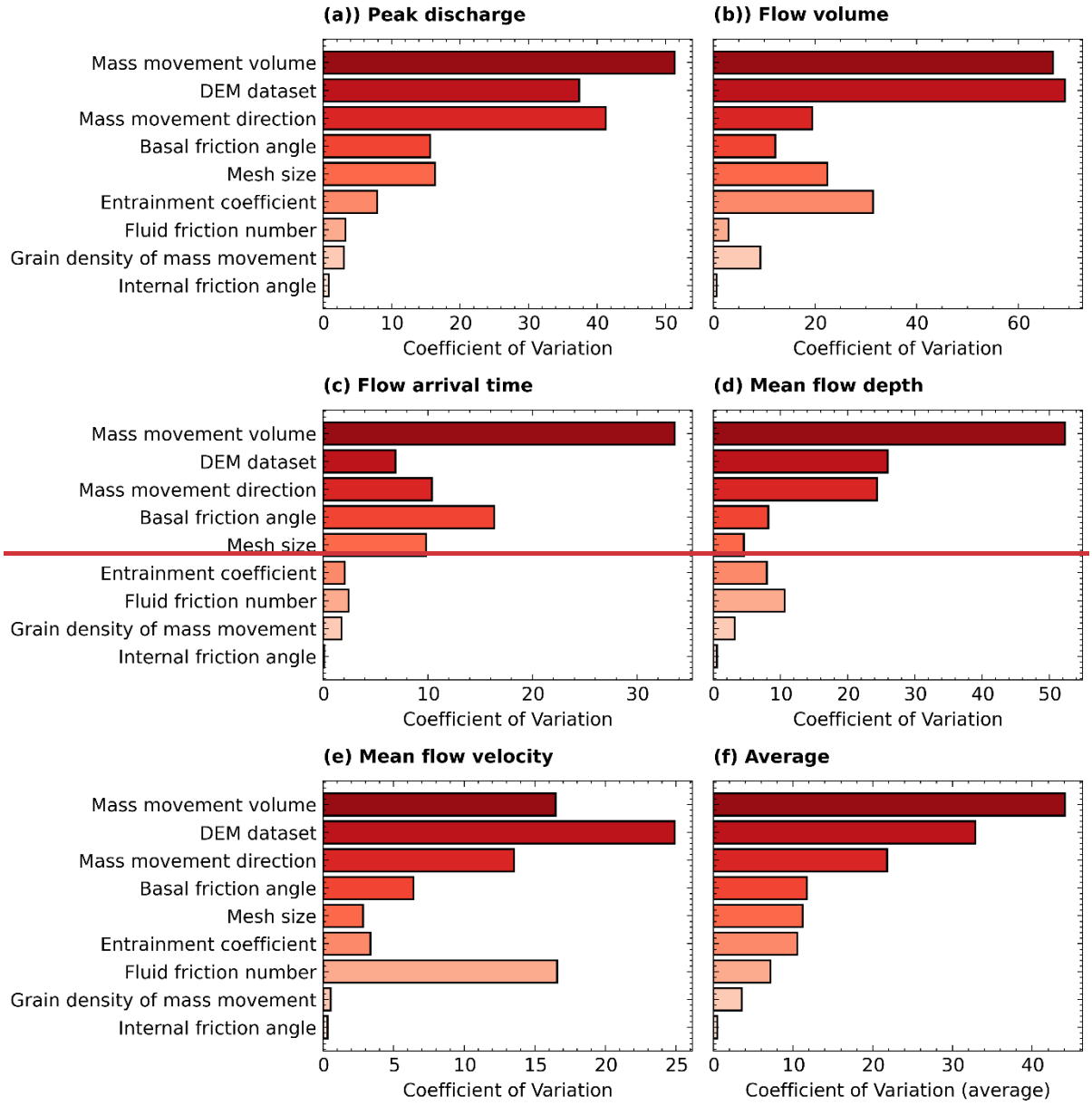

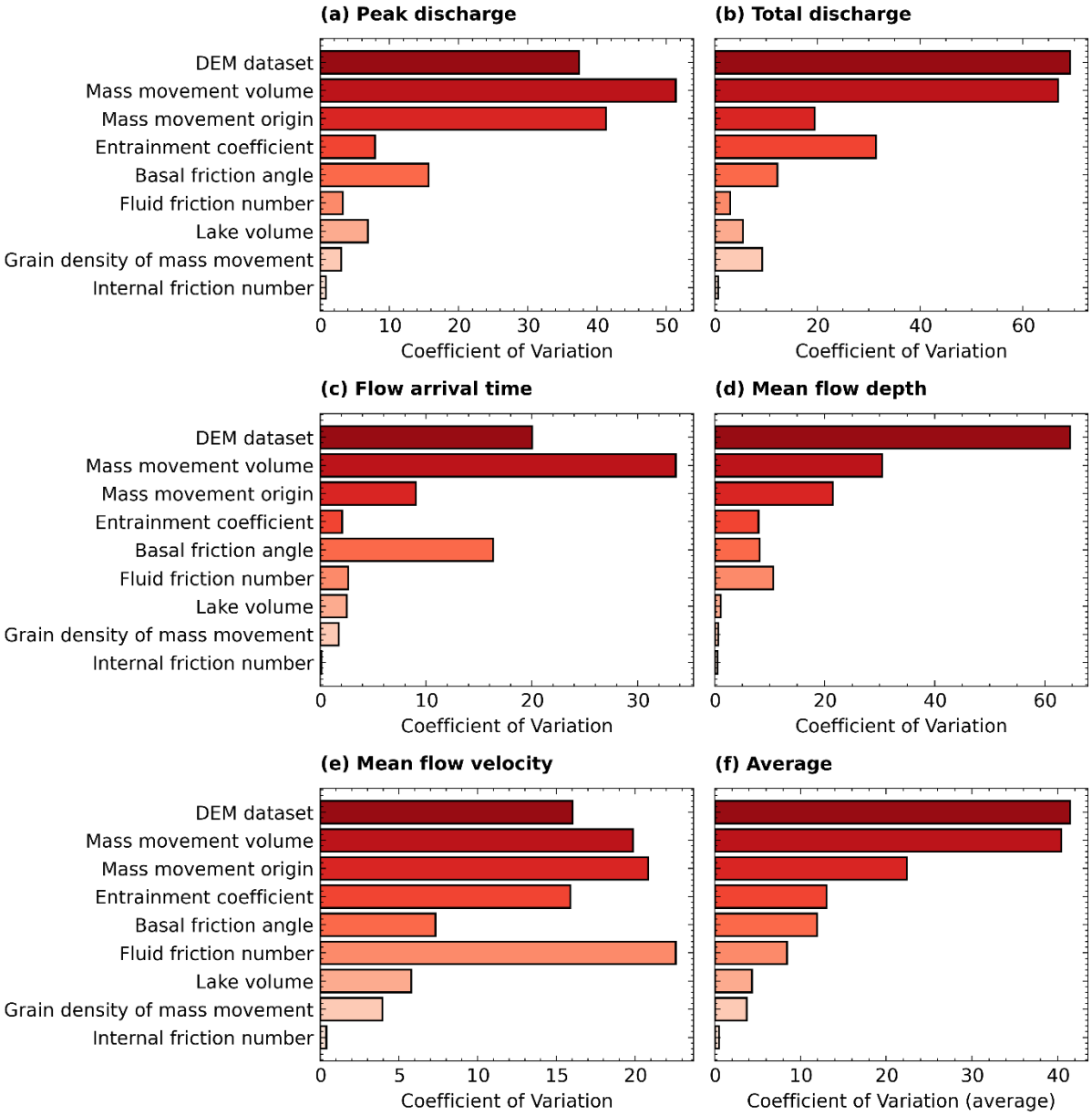

Figure 8: The coefficient of variation for (a) peak flow, (b)volume, (c) time, (d) average ~~flow height~~flow depth along the river centreline, (e) flow velocity along the river centreline and (f) average across all these output parameters.

4.~~7~~7 Comparison of the effects of all parameters

To compare output sensitivity resulting from all input parameters ~~and initial conditions~~ considered here, we calculated the percentage of coefficient of variation (CV) for peak flow, total discharge, arrival time, ~~flow height~~flow depth and flow velocity. We further computed the average ~~coefficient of variation~~CV (avg. CV) across all these output variables and examined the overall impact of each input parameter variation. Comparing all these output indicators, ~~mass movement~~V_S ~~entering the lake~~ had the greatest impact (avg. CV = 47%), followed by DEM datasets (avg. CV = 35%) and the origin of mass movement (avg. CV = 21%). Other

input parameters like ~~mesh size, basal friction angle (δ),~~ and ~~entrainment coefficient~~C_E also caused significant variation in resulting GLOFs. Notably, ~~fluid friction number~~C_{FF} ~~had a significant impact on~~significantly impacted ~~flow height~~flow depth with its CV = 16% despite having minimal impact on other flow characteristics.

For the ~~six~~ seven scalable parameters, we computed linear regression (Fig. 5 ~~to Fig. 7~~). The linear regression analysis ~~unveiled~~ revealed that the ~~four~~ five parameters~~:, namely~~ ~~volume (R^2=0.99) of mass movement~~V_S ~~into l~~ake (R^2 = 0.99), ~~ρS of mass movement~~ρS ~~into lake~~ (R^2=0.96), V_L (R^2 = 0.81), ~~basal friction angle (δ)~~ (R^2 = 0.96) and C_{FF} (R^2 = 0.83) ~~offer~~ demonstrated strong explanatory power ~~regarding~~ in accounting the variability ~~observed in resulting~~in GLOF peak discharge (Fig. 5). Among these sets of parameters, ~~volume~~V_S (m = 1.6), ~~and ρS (m = 0.085) of mass movement~~ρS (m = 0.085) ~~entering lake~~and V_L (m = 0.07), ~~indicated~~showed a positive relationship while δ (m = -0.347), ~~and~~ C_E (m=-0.091) and C_{FF} (m = -0.09) exhibited a negative relationship (Fig. 5). ~~By contrast, the internal friction angle (R^2 = 0.24) and entrainment coefficient (C_E) (R^2 = 0.22) exhibited a weak relationship with the peak discharge.~~ All ~~six~~ seven parameters (R^2 >0.~~8~~69) except for the ϕ ~~internal friction angle~~ (R^2 =0.59) and V_L (R^2= 0.25) indicated a high level of explanatory power regarding the variation of resulting total discharge (Fig. 6). Comparing all seven input parameters~~Across all six parameters~~, ~~the volume of the avalanche~~ V_S exhibited the highest R^2 value for both peak and total discharge, signifying a strong explanatory power regarding the modelled flow~~discharge volume~~ compared to the other parameters. Additionally, the rate of change of peak discharge and total discharge for every unit increase in V_S was comparatively higher than other parameters as indicated by the steepness of the slope ~~substantial magnitude of the slope (m=1.6 and m=0.53 for peak and total discharge, respectively) associated with the volume of avalanche further underscores its high magnitude relationship with the modelled GLOF flow, surpassing that of the other parameters~~ (Fig. 5a and 6a).

Basal friction angle ~~δ~~ and C_{FF} demonstrated a high level of explanatory power concerning the variability in flow arrival time, as evidenced by their R^2 values of 0.98 and 0.97, respectively. ~~Avalanche~~ Mass movement volume variation also exhibited a high explanatory power with a negative relationship, ~~supported by~~with ~~an~~ R^2 of 0.81 and a slope (m) of -0.019~~, although~~. However, the linearity became less pronounced within the volume range of 4 × 10^6 m^3 to 10 × 10^6 m^3. In contrast, other parameters, including C_E, and ϕ, did not exhibit a definitive linear relationship ~~.~~ (Fig. 7). However, C_E variation showed a threshold effect on arrival time; increasing the C_E from $10^{-5.95}$ to $10^{-6.42}$ kg^{-1} decreased arrival time, while further increases towards $10^{-5.85}$ kg^{-1} led to a linear increase in arrival time.

5 Discussion

Our primary aim was to investigate the sensitivity of the modelled GLOF outputs ~~from r.avaflow~~ to a range of values for key model input parameters using r.avaflow model. Previous studies have underscored the sensitivity of ~~r.avaflow~~GLOF model outputs to ~~various~~ some input parameters, including basal friction angle, entrainment coefficient and volume of ~~avalanche~~ mass movement entering the lake (Baggio et al., 2021; Mergili et al., 2018b; Mergili et al., 2020a). This study advances our understanding of GLOF modelling by conducting a comprehensive sensitivity analysis across nine essential parameters ~~-~~and multiple (84) GLOF simulations. As a result, we have for the first time, ranked these nine GLOF input parameters based on their contributions to model output variabilities. Our results showed that modelled GLOF output parameters are substantially sensitive to ~~six~~ five of the nine parameters we tested here (DEM dataset, ~~mesh size,~~ volume of mass movement into the lake, origin of mass movement into the lake, entrainment coefficient, and basal friction angle) suggesting that GLOF modelling results are subject to uncertainty from ~~the~~ multiple sources. The findings offer valuable perspectives on the uncertainty of GLOF modelling results and complexities inherent in modelling the GLOF process chain within the rugged mountain terrain such as in the Himalaya.

5.1 DEM datasets ~~and mesh size variations~~

DEM is one essential data for GLOF and other flood modelling (Hawker et al., 2018; Saksena and Merwade, 2015; Schumann and Bates, 2018; Westoby et al., 2014). The impact of DEM resolution is even more pronounced in the steep and complex topographic conditions prevalent in high mountain regions like the Himalaya (Liu et al., 2019). Our study provides the quantification of the effect of DEM in such environments for the first time. Our results suggest that the use of global and regional DEM datasets with resolution ranging from ~~HMA-DEM (~~8 m (HMA-DEM)~~)~~ to ~~SRTM GL3 (~~90 m~~)~~ (SRTMGL3) leads to over two-fold and four-fold variations in peak and total discharge, respectively, and cause successive significant fluctuations in flood height, reach distance and flow arrival time. This likely results from the low-resolution DEMs not fully resolving the river channel compared to ~~higher resolution~~higher-resolution ~~DEM~~DEMs. This limitation results in a reduction in~~, leading to~~ surface roughness and ~~reduced r~~river channel conveyance (carrying capacity of channel). Thus, the flow spreads out more, leading to an increase in the modelled flow extent and reach (Fig. 9 and Fig. S7) (Muthusamy et al., 2021). This was supported by ~~a comparison of~~comparing the DEM profile and ~~flow height~~flow depth along the river centreline (Fig. 9) and across the multiple vertical cross-sections along the river channel (Fig. S6). The analysis showed that GLOF output from ~~SRTM GL3~~SRTMGL3, where river channels are poorly resolved, was comparatively higher than that from the HMA-DEM with the ~~better resolved~~better-resolved channel. Also, DEM

datasets were acquired at different times, meaning the topographic features they captured ~~might also~~will also differ depending on natural geomorphological change or human-made alteration of the earth's surface over time (Khosh Bin Ghomash et al., 2019; Bishop et al., 2002; Schumann and Bates, 2018; Watson et al., 2015). Such discrepancies will have a substantial influence on flow characteristics and huge uncertainty if a DEM with inadequate spatial and temporal resolution is used in GLOF modelling.

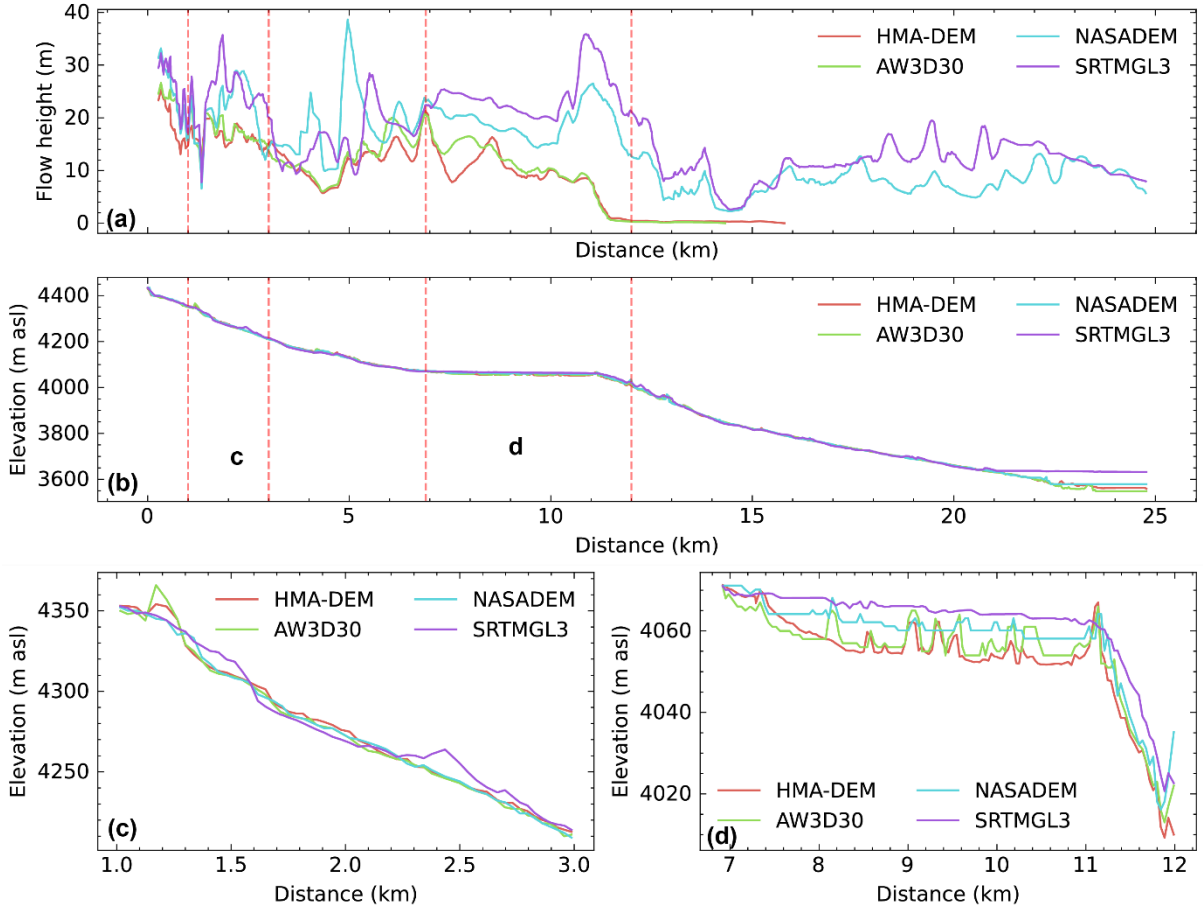

Figure 9: A comparison of the elevation profiles from four DEM datasets and the corresponding flow depths along the river centreline, generated through r.avaflow modelling. panels (a) and (b) show the flow depths and elevation profiles along the river centreline. Panels (c) and (d) illustrate elevation profiles for two specific sections marked in (a) and (b). DEM and ~~flow height~~flow depth profiles from the vertical cross sections at various distances are also provided in the supplementary figure (Fig. S6). The DEM datasets were co-registered using the algorithm developed by Shean et al. (2016).

Overestimation of flood maps stemming from reductions in DEM resolution has been reported in urban flood modelling (Muthusamy et al., 2021; Mcclean et al., 2020). However, the impact of DEM data on GLOF modelling, especially in a complex topographic setting such as in the Himalaya has been rarely documented (Wang et al., 2011). Our results show the substantial

variation in GLOF model output stemming from DEM dataset variation, even when employing DEM with comparable spatial resolutions, ~~which~~ underscores the criticality of high-quality DEM data in GLOF modelling (Fig. 9). DEM datasets covering rugged high mountain terrain, where GLOFs typically occur are likely to have more errors due to geometric distortion and data loss due to challenges involved in data acquisition for DEM production (Hugonnet et al., 2021; Liu et al., 2019). Therefore, using global to regional scale open-access ~~-~~DEMs, such as SRTM for GLOF modelling due to the absence of high-resolution alternatives (Wang et al., 2011) may only be suitable for first-order assessment of GLOFs at large scales (Zhang et al., 2023b). This is important as uncertainty stemming from DEM datasets is often overlooked and/or not well addressed in the previous basin-specific GLOF modelling work (Rinzin et al., 2023; Sattar et al., 2023; Sattar et al., 2021b).

5.2 Mass movement origin variation

Our study indicated that different ~~locations~~ origin of ~~avalanche~~ mass movement initiation produced GLOFs with approximately two-fold variations in their peak discharge, volume, and reach distance (Fig. 4). These variations can be explained based on the lake geometry and the direction, horizontal distance and vertical distance ~~/ angle~~ at which the mass movement enters the lake. r.avaflow model provides detailed output parameters such as kinetic energy associated with the flow, and flow ~~height~~ depth map for each time step, which allowed us to better understand the cause of this variation. For example, the ~~avalanche~~ mass movement~~mass~~ originating from L~~l~~oc-1, which is located at the slope above the headwall, directly impacts the head end of the lake with the highest kinetic energy (50714 GJ) among all other ~~source~~sources of ~~avalanches~~mass movement. This head-end impact, coupled with its high energy, facilitates the direct forward propagation of waves toward the frontal outlet, causing the lake water to overtop the frontal moraine and resulting in a higher peak and total discharge (Fig. S7). Thorthormi Tsho is roughly crescentic in shape and curves toward the west, with its maximum curvature facing the mass movement origin of L~~l~~oc-5~~6~~. This shape also allows the impact wave generated from mass movement from ~~l~~Loc-5~~6~~ to move almost unimpeded along the flow line, resulting in greater GLOF discharge. Also, Loc-1 and Loc-5 are located at greater distances and higher elevations from the lake compared to other locations (Fig. 2). This spatial location might have also enabled them to generate greater force to impact the lake. In contrast, the direct wave of impact generated by the mass movement from L~~l~~oc-3, located on the slope above the right moraine dam, is deflected towards the left lateral moraine, and only a secondary wave proceeds towards the lake outlet, resulting in a comparatively lower peak and total discharge (Fig. S7) (Emmer et al., 2024). This finding implies that the geometry of the glacial lake and the surrounding source slope plays a vital

role in GLOF output. Thus, we underscore the importance of considering catchment shape in GLOF modelling, although we cannot assume that two identical basins will have the same flood properties due to the influence of other factors, such as the involved volume of solid and fluid parts.

Earlier studies (Mergili et al., 2017; Mergili et al., 2020b) have explained the interaction between landslides and reservoirs (lakes) and their influence on the resulting hydrograph. However, these studies did not consider the variables such as directions ~~and angles~~and distances from which the mass impacts the lake. To fill this gap, here we enhanced our understanding of the interplay between the resulting GLOF magnitude and ~~avalanche~~ mass movement attributes including the direction and ~~angle~~ distance from which the ~~avalanche~~ mass enters the lake, the amount of kinetic energy the ~~avalanche~~ mass possesses and the geometry of the lake. Our results emphasize the significant impact on the resulting GLOF events caused by the uncertainty in pinpointing the specific location of origin of mass movement into the lake. Thawing of permafrost and destabilization of the slope surrounding the lake due to climate warming (Gruber et al., 2017; Kääb et al., 2018; Sattar et al., 2025) combined with the expansion of the glacial lake towards the mountain flank (Rounce et al., 2016) are likely to increase the frequency of mass movement into the lake, further exacerbating this uncertainty. By effectively identifying and quantifying the uncertainties related to the origin of mass movement entering the lake in addition to the volume, we propose considering the origins of mass movement in designing the scenario-based GLOF modelling in future studies. This approach goes beyond the existing practice, which primarily focuses on the volume of mass movement entering the lake. This is important because, as demonstrated in our study, the impact of mass movement can vary significantly depending on its origin. In some cases, what may be considered a worst-case scenario from one origin might represent only a low-magnitude event from another ~~Therefore, our finding here will be useful to further improve the development of scenario-based approaches to GLOF modelling~~ (Gaphaz, 2017; Sattar et al., 2021a; Allen et al., 2022)~~ including, high, medium, small and worst-case scenarios (Allen et al., 2022; Gaphaz, 2017)~~.

~~5.3 Mass~~5.3 Mass movement volume, grain density, ~~and~~ entrainment coefficient, and lake volume

Our investigation revealed that variation in GLOF magnitude is most sensitive to the volume of ~~avalanches~~ mass movement (V_S) entering the lakes. It also exhibits a significant level of sensitivity to the entrainment coefficient (~~whilst~~C_E) whilst the grain density (ρS) and lake volume (V_L) exhibit~~s~~ negligible impact. For example, the variation of ~~avalanche~~ V_S~~volume~~ between 1×10^6 m^3 and 10×10^6 m^3 leads to peak and total discharge fluctuation of 1160% and

2500%, respectively, and subsequent variation in maximum ~~flow height~~flow depth and arrival time (Fig. 5 to Fig. 7). The dominant impact of ~~avalanche~~ V_S~~volume~~ and ~~entrainment coefficients~~C_E on GLOF magnitude could be due to their direct influence on the overall magnitude and intensity of flood events. The total discharge during the GLOF cascade event is a function of the ~~volume of the avalanche~~ V_S entering the lake. This is further corroborated by the near-perfect linear relationship ~~between~~ of peak discharge (R^2 = 0.99) and total discharge (R^2 = 1) with the ~~volume of avalanches~~ V_S entering the lake observed here. Likewise, the volume of solid content in the flow is solely contributed by the entrainment of frontal moraine material, primarily determined by the ~~entrainment coefficient (~~C_E~~)~~. Additionally, this correlation could be attributed to the amount of energy and associated momentum of the flow, which changes significantly with corresponding variations in ~~avalanche~~ V_S~~volume~~. Also, it could be due to the longer timing and duration of the flow as evident in Fig. S24. Most GLOF events in high mountains across the HMA and other alpine regions are caused by moraine dam breaches triggered by mass movement entering the lake from the surrounding mountain flank (Shrestha et al., 2023; Lützow et al., 2023; Emmer and Vilímek, 2014). As a result, ~~mass movement volume~~V_S is considered a primary basis for scenario development (Allen et al., 2022). Thus, we believe this finding provides useful insights towards improving the ~~developing~~ development of different scenarios of GLOFs with higher confidence, or is a basis for ensemble testing, with the caveat that the range of outputs may be too wide to be of practical use.

The volume of a glacial lake is one of the key parameters in GLOF modelling **and subsequent hazard mapping.** Without field-measured bathymetry, **we applied eight different empirical equations to estimate the volume of Thorthormi Tsho, which ranged between 2.1 and 3.80 × 10⁸ m³. Interestingly, this variation in** V_L **did not significantly influence the** modelled **GLOF hydraulics;** V_L **was ranked as the third least sensitive parameter in our analysis. This limited impact may be attributed to the large size of Thorthormi Tsho (~4.35 km²) and its substantial storage capacity, as estimated by the empirical equations. Even the lower bound of the calculated** V_L **exceeds** 95% of the measured **volume** of the glacial lake and the upper bound is greater than 58 of the 59 measured volume of the lake in the **greater** Himalaya (Zhang et al., 2023a). We believe **that the** Thorthormi Tsho's **large volume and expansive area enable it to absorb and dissipate the energy from potential mass movement impacts, effectively acting as a buffer** (Emmer et al., 2024)**. Nevertheless, while our findings suggest that** V_L **uncertainty may have a relatively minor impact on GLOF** modelling **for large lakes like Thorthormi Tsho, we acknowledge that** V_L **remains a critical parameter in GLOF** modelling**, particularly for**

smaller lakes where volume changes could have a more pronounced effect on flood dynamics (Sattar et al., 2023).

5.4 Frictional parameters variations

Among the frictional parameters, our result showed that GLOF magnitude is most sensitive to the basal friction angle (δ). For example, the variation of total discharge (47.5%) resulting from fluctuation of δ within the ~~conservative~~ experiment range was 30 times greater than that of internal friction angle (ϕ) and over four times greater than that of fluid friction angle (C_{FF}). δ plays a dominant role in flow dynamics and the interaction between the flowing material and the channel bed. This direct contact means that even minor changes in δ can have substantial effects on the resistance encountered by the flowing material, thereby influencing the mobility of the flow (Pudasaini and Krautblatter, 2014a; Mergili et al., 2018a; Mergili et al., 2018b). ϕ on the other hand primarily affects particle interactions within the flowing material, whilst C_{FF} is a coefficient which quantifies the overall flow resistance within the flow path mainly depending on surface roughness. Our findings indicate that prioritizing the consideration of δ over the other two frictional parameters is advisable. While the back-calculated values might seem reasonable initiation values for δ as measuring it in the field is practically not feasible we recommend conducting a statistically substantial sensitivity analysis using adequate sampling size and an appropriate statistical model. ~~This can be done by determining spatially variable values through field data con penetration test (). In the case where conducting field work is not possible,or conducting a statistically substantial sensitivity analysis. Nonetheless, d~~Despite the relatively low overall impact on GLOF magnitude, the C_{FF} notably increased the flow's mobility, especially beyond 12 km downstream, when the flow became fluid-dominant (Fig. S4). This is because C_{FF} ~~is controls~~controls the mobility of the fluid part (Mergili and Pudasaini, 2024~~b~~; Mergili et al., 2017). This suggests that C_{FF} could exert a substantial influence, particularly in modelling scenarios encompassing longer flow distances.

5.5 Key points from the comparison of all parameters and the way forward

Identifying the most accurate parameter values or optimal datasets can be achieved through validation with well-constrained historical events (Zheng et al., 2021a; Schneider et al., 2014; Mergili et al., 2020b; Shugar et al., 2021; Sattar et al., 2025), but there are limitations in the transferability of these findings due to ~~the~~ unique characteristics and initial conditions of each GLOF, such as varying ~~volumes~~ proportions of ~~of~~ solid and liquid parts. Because of this we effectively constrained how variation in input parameter values within commonly used ranges,

influences the GLOF modelling results, instead of trying to determine the 'correct' value for each parameter. Or, put another way, if we apply our study to a specific example, we may determine that certain factors are more important than others for this specific example, but it would be unclear how applicable our results are to other events. Thus, we see our approach as the least biased towards any particular event and hence the most generally applicable approach. Our results indicating modelled GLOF being subjected to uncertainty from multiple input parameters ~~These specific conditions mean that the~~implies that ~~results~~ parameter value determined from~~of~~ one modelled GLOF event might not accurately predict the behaviour of GLOFs in different regions or under different circumstances (Mergili et al., 2018a; Mergili et al., 2020b). Therefore, while these back-analysed parameter values can provide valuable insights, they need to be applied with caution and adapted to the specific context of each new GLOF scenario. ~~This is emphasized by our finding that the characteristics of the modelled GLOF are substantially impacted by various parameters.~~ As a result of these multiple sources of uncertainty in modelled GLOF, it could pose challenges in effectively communicating risks with communities and other stakeholders (Thompson et al., 2020). We highlight that more sensitive parameters should be treated carefully in future GLOF modelling works by robustly considering associated uncertainties.

Due to the high sensitivity of the model output on DEM resolution, we emphasize the critical importance of high-resolution and good-quality DEM (Uuemaa et al., 2020; Schumann and Bates, 2018), especially when modelling is aimed at producing hazard maps with higher granularity at the specific basin scale. ~~Specifically,~~ DEMs should be ~~the~~ high spatial resolution, high vertical accuracy and recently produced, especially in areas of high relief and rapid landscape change such as in Himalaya (Schumann and Bates, 2018). Previous studies have indicated that flood modelling accuracy can be improved by correcting the effect of DEM resolution and accuracy (Saksena and Merwade, 2015) or by merging with other high-resolution and accurate DEMs (Muthusamy et al., 2021). These methods appear viable in the context of highly sparse coverage of high-resolution DEMs and the unaffordability of high-resolution commercial DEMs, but the modelling results ~~should still be interpreted with caution~~may be subjected to substantial uncertainty. ~~On the other hand, whilst it poses computational challenges, especially with high-resolution DEMs, we believe that selecting a mesh size equivalent to the spatial resolution of the DEM could effectively mitigate uncertainty associated with mesh size variation. Models such as D-Claw which features patch-based adaptive mesh refinement capability can be potentially used as alternative models, however, its use in GLOF modelling is limited so far (Iverson and George, 2014; George et al., 2017).~~

~~Avalanche~~ Mass movement volume and δ exhibit a strong linear relationship with all output parameters. Whilst the linear relationship does not negate the influence these parameters have on flow ~~characteristics,~~characteristics; it suggests that model output errors resulting from uncertainties in these parameters might be predictable~~ly managed~~. This is essential since predicting the ~~volume of mass~~V_S movement involved in the forward modelling is highly challenging and determining an accurate value is impossible – the current challenge is rather to establish a likely envelope of volumes. However, such prediction should be bespoke to the particular events based on the initial parameters like estimated ice thickness, slope, and presence of permafrost. Furthermore, such predictions must also consider other factors, such as equifinality arising from the interaction of multiple parameters (Mergili et al., 2018a; Mergili et al., 2018b; Mergili et al., 2020b).

The entrainment coefficient exhibits a threshold effect for peak discharge, arrival time and total discharge but these thresholds occur at different C_E values for each of these output parameters. ~~The C_E exhibits a linear relationship only with volume.~~This ~~effect might be a~~consequence ~~This relationship with the volume is understandable, as the entrainment coefficient is a primary determinant of how much solid fraction of the flow is added due to erosions.~~The observed threshold effects in flow characteristics can likely be attributed to the initial dominance of the fluid component, wherein the contribution of erosion to the flow dynamics is negligible. As the erosion rate progresses with increasing CE values, the increasing concentration of eroded material reduces the mobility of the flow, leading to a decline in mobility of the flow~~further the solid components of the mobility However, the arrival time exhibits distinct thresholds at the entrainment coefficient $10^{-6.46}$ kg^{-1}. The decrease in flow arrival time observed until a C_E value of $10^{-6.46}$ kg^{-1} may be attributed to the flow being primarily dominated by the fluid component, with the contribution from erosion being negligible. However, the subsequent increase in flow arrival time as the C_E value further increased from $10^{-6.46}$ kg^{-1} to $10^{-5.85}$ kg^{-1} could be attributed to the effect of increasing concentration resulting from a higher rate of erosion~~less mobile. ~~These threshold effects~~is suggest~~s~~ that once these~~is~~ thresholds ~~is~~ are surpassed, the resulting ~~peak~~ flow and arrival time demonstrate a heightened sensitivity to variations in entrainment. Consequently, this sensitivity may translate to the flow characteristics such as ~~flow height~~flow depth and ~~arrival and~~ arrival time which are essential for hazard and risk assessments. It is important to note that this threshold value may vary across different GLOF events due to the diverse combinations of other parameters.

~~The linearity demonstrated by the initial volume of avalanches entering the lake and δ warrants further investigation into flow characteristics resulting from variations in these parameters. Further investigation with adequate sample sizes and a reliable statistical approach would~~

~~enable the establishment of accurate relationships or predictor values. The threshold effect observed in the C_E value also warrants further investigation using statistically conclusive samples to determine whether the threshold value is universal across different events or specific to individual occurrences. For factors such as internal friction angle, fluid friction number, and ρS, the conservative values may suffice or receive less emphasis, particularly considering the numerous parameters involved in GLOF modelling.~~

~~The r.avaflow model provides comprehensive and open-source codes for simulating cascading mass flow in complex topographies~~ (Mergili and Pudasaini, 2024a)~~. Its comprehensiveness stems from the wide range of parameters it considers, making it a versatile tool for various mass flow process chain simulations (Mergili et al., 2017). Past studies have demonstrated the model's ability to accurately back-calculate historical events with detail (Shugar et al., 2021). However, challenges persist in its application to forward modelling (Allen et al., 2022; Sattar et al., 2023), particularly in the context of GLOF hazard and risk assessment (Mergili et al., 2020b). In our study, we conducted a robust sensitivity analysis considering nine parameters relevant to GLOF towards addressing these challenges. Since we identified the key parameters that significantly influence the modelled GLOF output, our result can be used as a basis for further improvement and optimization of r.avaflow modelling codes.~~

~~The~~The GLOF simulations were conducted using the r.avaflow model due to its capability to model the entire GLOF process chain (Mergili and Pudasaini, 2024~~b~~; Mergili et al., 2017). While we present the uncertainty involved in the full process chain GLOF from mass movement entering the lake to downstream propagation, we specifically explored the uncertainty of the GLOF input parameters relevant to r.avaflow modelling. Input parameters such as DEM datasets, and the volume and density of mass movement involved in a GLOF event, might be similar across different models. However, it should be noted ~~we caution~~ that ~~the~~ all ~~lhe~~ parameters tested here do not necessarily apply to all models used for GLOF modelling.

The flow arrival time was measured from the profile located 3 km, 6 and 9 km downstream of the lake since some of our modelled GLOF terminates before proceeding further downstream. This is a reasonable point as human settlement downstream of the lake is mostly concentrated around this area. The variation of flow arrival time might be underestimated if the location is farther downstream from the lake.

Here we focused on nine essential parameters in r.avaflow, which are relevant to GLOF modelling. As an open-source modelling code, r.avaflow model offers flexibility by allowing

the users to manipulate all parameters, a level of transparency that sets it apart from many modelling codes. However, including inbuilt modules, initial conditions, and all flow parameters, r.avaflow has more than 30 tuneable parameters (Mergili and Pudasaini, 2024~~b~~) (Table S1). Our choice of parameter in this study is essentially motivated by those identified as critical and commonly modified in the previous GLOF modelling studies and which are frequently modified to fit with the parameter from back-calculated events. Because of~~Thus, ou these~~this, ~~r~~our ~~-~~sensitivity analysis might have potentially overlooked the complexity of r.avaflow stemming from the effect of all these parameters, let alone their interaction effect.

Also due to the enormous computational time and resources required for running r.avaflow, we used one-at-a-time sensitivity analysis conducting up to 10 simulations per parameter.~~One-at-a-time sensitivity analysis we used here, inherently lacks consideration for parameter interactions and may have potentially overlooked important relationships (Saltelli et al., 2004). Moreover, due to the immense computational cost of r.avaflow, we used only 10 simulations.~~ While this number of simulations for each parameter produced substantially conclusive results, we do not discount the robustness of global sensitivity analysis employing an adequate sampling size which can adequately account for the influence of parameter interactions (Saltelli et al., 2004). While we offer for the first time the importance of considering the uncertainty of these parameters in GLOF modelling, in the light of all these limitations, we provide the following recommendations: 1) We recommend that future studies include a broader range of parameters, further advancing the understanding of their roles in GLOF modelling: 2) ~~Future~~ This can be achieved by initially focusing on the most sensitive parameters identified in this study and progressively expanding the analysis to include other parameters. Adequate sample sizes and appropriate statistical models should be employed to ensure robust findings~~studies should focus on testing further r.avaflow parameters and in-depth model analysis by employing a statistically sufficient sampling size~~: 3) ~~.~~Given that r.avaflow is an open-source tool under continuous development, we underscore the implementation of features that support parallel computation for parameter interaction analyses. This advancement would enable future studies to fully utilize high-performance computing (HPC) resources and address complex modelling challenges more effectively.

6 Conclusions

GLOFs present substantial dangers to communities residing in valleys downstream of glacial lakes. GLOFs involve complex cascading processes and typically occur across rugged mountain terrains. Due to these complexities, modelling GLOFs necessitates extensive input data, parameters, and complex modelling codes for accurate hazard and risk assessments, which is inherently challenging. However, previous studies have mostly relied on open-access

data and are grounded in a historical event introducing significant uncertainties to the modelling results. In this study, we have, for the first time, conducted sensitivity analysis considering multiple GLOF parameters and ranked these inputs based on how their uncertainties in input values apportion to the variation in modelling output, by employing cutting-edge modelling code, r.avaflow. Our results suggested GLOF modelling outputs such as peak and total discharge are substantially sensitive to variation in input values of six out of nine parameters we tested here. Specifically, the modelling outputs are the most sensitive to the volume of ~~avalanches~~ mass movement entering lakes followed by the variation in DEM datasets and the location of origin of mass movement entering the lake. Other parameters like ~~mesh size~~, basal frictional angle ~~,~~ and entrainment coefficient also showed significant sensitivity. Although limited to GLOF modelling with the r.avaflow model, our study emphasizes that GLOF modelling results are influenced by uncertainties stemming from various sources, underscoring the need for careful interpretation of the modelling results. By ranking the model parameters according to their impact on model output, our study prioritizes model input parameters for future modelling efforts, given the challenge of adequately constraining multiple parameters. Additionally, this study lays the groundwork for a thorough investigation into the most sensitive parameters, to improve our understanding of GLOF modelling.

Acknowledgement

This work was supported by the Natural Environment Research Council (NERC)- funded IAPETUS Doctoral Training Partnership [IAP2-21-267]. We thank Dr. Sonam Wangchuk of ICIMOD for helping us in setting experiment in the HPC.

Code and data availability

The r.avaflow modelling code we used here for simulating all scenarios of GLOF can be accessed at: r.avaflow | The mass flow simulation tool (landslidemodels.org). The ~~SRTM GL3~~SRTMGL3, NASADEM and AW3D30 DEMS used here can be downloaded from the OpenTopogragphy at: OpenTopography - Find Topography Data. The HMA-DEM can be downloaded from the National Ice and Snow Data Center at: High Mountain Asia 8-meter DEM Mosaics Derived from Optical Imagery, Version 1 | National Snow and Ice Data Center (nsidc.org).

Supplement

The supplement related to this article is available online at:

Author contributions

SR, SA~~.~~ and RC conceptualized the study. SR undertook the ~~computational studies~~data and data processing and analysis. SA and RC secured the funding, supervised, and contributed equally to the work. AS helped~~provided guidiance in~~ modelling and was involved as an external supervisor. MM revised and ~~provide~~ provided an expert opinion on the study~~. SA, RC and AS supervised the work~~. All authors wrote and ~~edited~~ revised the manuscript.

Competing interests

The contact author ~~has declared~~ declares that none of the authors has any competing interests.

References

(SRTM), N. S. R. T. M.: Shuttle Radar Topography Mission (SRTM) Global [dataset], https://doi.org/10.5069/G9445JDF, 2013.

Abdi, H.: Coefficient of variation, Encyclopedia of research design, 1, 2010.

Allen, S. K., Zhang, G., Wang, W., Yao, T., and Bolch, T.: Potentially dangerous glacial lakes across the Tibetan Plateau revealed using a large-scale automated assessment approach, Science Bulletin, 64, 435-445, 10.1016/j.scib.2019.03.011, 2019.

Allen, S. K., Linsbauer, A., Randhawa, S. S., Huggel, C., Rana, P., and Kumari, A.: Glacial lake outburst flood risk in Himachal Pradesh, India: an integrative and anticipatory approach considering current and future threats, Natural Hazards, 84, 1741-1763, 10.1007/s11069-016-2511-x, 2016.

Allen, S. K., Sattar, A., King, O., Zhang, G., Bhattacharya, A., Yao, T., and Bolch, T.: Glacial lake outburst flood hazard under current and future conditions: worst-case scenarios in a transboundary Himalayan basin, Natural Hazards and Earth System Sciences, 22, 3765-3785, 10.5194/nhess-22-3765-2022, 2022.

Baggio, T., Mergili, M., and D'Agostino, V.: Advances in the simulation of debris flow erosion: The case study of the Rio Gere (Italy) event of the 4th August 2017, Geomorphology, 381, 10.1016/j.geomorph.2021.107664, 2021.

Bishop, M. P., Shroder, J. F., Bonk, R., and Olsenholler, J.: Geomorphic change in high mountains: a western Himalayan perspective, Global and Planetary Change, 32, 311-329, https://doi.org/10.1016/S0921-8181(02)00073-5, 2002.

Buckley, S., Agram, P., Belz, J., Crippen, R., Gurrola, E., Hensley, S., Kobrick, M., Lavalle, M., Martin, J., and Neumann, M.: NASADEM, National Aeronautics and Space Administration, Jet Propulsion Laboratory, California Institute of Technology: Pasadena, CA, USA, 2020.

Byers, A. C., Rounce, D. R., Shugar, D. H., Lala, J. M., Byers, E. A., and Regmi, D.: A rockfall-induced glacial lake outburst flood, Upper Barun Valley, Nepal, Landslides, 16, 533-549, 10.1007/s10346-018-1079-9, 2018.

Carrivick, J. L. and Tweed, F. S.: A global assessment of the societal impacts of glacier outburst floods, Global and Planetary Change, 144, 1-16, 10.1016/j.gloplacha.2016.07.001, 2016.

Dubey, S. and Goyal, M. K.: Glacial Lake Outburst Flood Hazard, Downstream Impact, and Risk Over the Indian Himalayas, Water Resources Research, 56, 10.1029/2019wr026533, 2020.

Dubey, S., Sattar, A., Goyal, M. K., Allen, S., Frey, H., Haritashya, U. K., and Huggel, C.: Mass Movement Hazard and Exposure in the Himalaya, Earth's Future, 11, 10.1029/2022ef003253, 2023.

Emmer, A. and Cochachine, L.: The causes and mechanisms of moraine-dammed lake failures in the Cordillera blanca, North American Cordillera, and Himalayas, AUC Geographica, 48, 10, 2013.

Emmer, A. and Vilímek, V.: New method for assessing the susceptibility of glacial lakes to outburst floods in the Cordillera Blanca, Peru, Hydrology and Earth System Sciences, 18, 3461-3479, 10.5194/hess-18-3461-2014, 2014.

Emmer, A., Vilca, O., Salazar Checa, C., Li, S., Cook, S., Pummer, E., Hrebrina, J., and Haeberli, W.: Causes, consequences and implications of the 2023 landslide-induced Lake Rasac GLOF, Cordillera Huayhuash, Peru, EGUsphere [preprint], 10.5194/egusphere-2024-2316, 2024.

Farinotti, D., Huss, M., Fürst, J. J., Landmann, J., Machguth, H., Maussion, F., and Pandit, A.: A consensus estimate for the ice thickness distribution of all glaciers on Earth, Nature Geoscience, 12, 168-173, 10.1038/s41561-019-0300-3, 2019.

Frey, H., Huggel, C., Chisolm, R. E., Baer, P., McArdell, B., Cochachin, A., and Portocarrero, C.: Multi-Source Glacial Lake Outburst Flood Hazard Assessment and Mapping for Huaraz, Cordillera Blanca, Peru, Frontiers in Earth Science, 6, 10.3389/feart.2018.00210, 2018.

Fujita, K., Sakai, A., Takenaka, S., Nuimura, T., Surazakov, A. B., Sawagaki, T., and Yamanokuchi, T.: Potential flood volume of Himalayan glacial lakes, Natural Hazards and Earth System Sciences, 13, 1827-1839, 10.5194/nhess-13-1827-2013, 2013.

Gantayat, P., Sattar, A., Haritashya, U. K., Watson, C. S., and Kargel, J. S.: Bayesian Approach to Estimate Proglacial Lake Volume (BE-GLAV), Earth and Space Science, 11, 10.1029/2024ea003542, 2024.
GAPHAZ: Assessment of Glacier and Permafrost Hazards in Mountain Regions. Technical Guidance Document, Standing Group on Glacier and Permafrost Hazards in Mountains (GAPHAZ) of the International Association of Cryospheric Sciences (IACS) and the International Permafrost Association (IPA). 72, 2017.
Gruber, S., Fleiner, R., Guegan, E., Panday, P., Schmid, M.-O., Stumm, D., Wester, P., Zhang, Y., and Zhao, L.: Review article: Inferring permafrost and permafrost thaw in the mountains of the Hindu Kush Himalaya region, The Cryosphere, 11, 81-99, 10.5194/tc-11-81-2017, 2017.
Hawker, L., Bates, P., Neal, J., and Rougier, J.: Perspectives on Digital Elevation Model (DEM) Simulation for Flood Modeling in the Absence of a High-Accuracy Open Access Global DEM, Frontiers in Earth Science, 6, 10.3389/feart.2018.00233, 2018.
Huggel, C.: Recent extreme slope failures in glacial environments: effects of thermal perturbation, Quaternary Science Reviews, 28, 1119-1130, 10.1016/j.quascirev.2008.06.007, 2009.
Hugonnet, R., McNabb, R., Berthier, E., Menounos, B., Nuth, C., Girod, L., Farinotti, D., Huss, M., Dussaillant, I., Brun, F., and Kaab, A.: Accelerated global glacier mass loss in the early twenty-first century, Nature, 592, 726-731, 10.1038/s41586-021-03436-z, 2021.
JAXA, J. A. E. A.: ALOS World 3D 30 meter DEM (V3.2), OpenTopography [dataset], 2021.
Kääb, A., Leinss, S., Gilbert, A., Bühler, Y., Gascoin, S., Evans, S. G., Bartelt, P., Berthier, E., Brun, F., Chao, W.-A., Farinotti, D., Gimbert, F., Guo, W., Huggel, C., Kargel, J. S., Leonard, G. J., Tian, L., Treichler, D., and Yao, T.: Massive collapse of two glaciers in western Tibet in 2016 after surge-like instability, Nature Geoscience, 11, 114-120, 10.1038/s41561-017-0039-7, 2018.
Khosh Bin Ghomash, S., Caviedes-Voullieme, D., and Hinz, C.: Effects of erosion-induced changes to topography on runoff dynamics, Journal of Hydrology, 573, 811-828, 10.1016/j.jhydrol.2019.04.018, 2019.
Lala, J. M., Rounce, D. R., and McKinney, D. C.: Modeling the glacial lake outburst flood process chain in the Nepal Himalaya: reassessing Imja Tsho's hazard, Hydrology and Earth System Sciences, 22, 3721-3737, 10.5194/hess-22-3721-2018, 2018.
Linsbauer, A., Paul, F., Machguth, H., and Haeberli, W.: Comparing three different methods to model scenarios of future glacier change in the Swiss Alps, Annals of Glaciology, 54, 241-253, 10.3189/2013AoG63A400, 2017.
Linsbauer, A., Frey, H., Haeberli, W., Machguth, H., Azam, M. F., and Allen, S.: Modelling glacier-bed overdeepenings and possible future lakes for the glaciers in the Himalaya—Karakoram region, Annals of Glaciology, 57, 119-130, 10.3189/2016AoG71A627, 2016.
Liu, K., Song, C., Ke, L., Jiang, L., Pan, Y., and Ma, R.: Global open-access DEM performances in Earth's most rugged region High Mountain Asia: A multi-level assessment, Geomorphology, 338, 16-26, 10.1016/j.geomorph.2019.04.012, 2019.
Lützow, N., Veh, G., and Korup, O.: A global database of historic glacier lake outburst floods, Earth Syst. Sci. Data Discuss., 2023, 1-27, 10.5194/essd-2022-449, 2023.
McClean, F., Dawson, R., and Kilsby, C.: Implications of Using Global Digital Elevation Models for Flood Risk Analysis in Cities, Water Resources Research, 56, 10.1029/2020wr028241, 2020.
Mergili, M. and Pudasaini, S. P.: r.avaflow - The mass flow simulation tool. r.avaflow.direct Web interface, 2024a.
~~Mergili, M. and Pudasaini, S. P.: r.avaflow - The mass flow simulation tool. r.avaflow.direct Web interface.,~~
Mergili, M., Fischer, J.-T., Krenn, J., and Pudasaini, S. P.: r.avaflow v1, an advanced open-source computational framework for the propagation and interaction of two-phase mass flows, Geoscientific Model Development, 10, 553-569, 10.5194/gmd-10-553-2017, 2017.

Mergili, M., Jaboyedoff, M., Pullarello, J., and Pudasaini, S. P.: Back calculation of the 2017 Piz Cengalo–Bondo landslide cascade with r.avaflow: what we can do and what we can learn, Natural Hazards and Earth System Sciences, 20, 505-520, 10.5194/nhess-20-505-2020, 2020a.
Mergili, M., Frank, B., Fischer, J.-T., Huggel, C., and Pudasaini, S. P.: Computational experiments on the 1962 and 1970 landslide events at Huascarán (Peru) with r.avaflow: Lessons learned for predictive mass flow simulations, Geomorphology, 322, 15-28, 10.1016/j.geomorph.2018.08.032, 2018a.
Mergili, M., Pudasaini, S. P., Emmer, A., Fischer, J.-T., Cochachin, A., and Frey, H.: Reconstruction of the 1941 GLOF process chain at Lake Palcacocha (Cordillera Blanca, Peru), Hydrology and Earth System Sciences, 24, 93-114, 10.5194/hess-24-93-2020, 2020b.
Mergili, M., Emmer, A., Juricova, A., Cochachin, A., Fischer, J. T., Huggel, C., and Pudasaini, S. P.: How well can we simulate complex hydro-geomorphic process chains? The 2012 multi-lake outburst flood in the Santa Cruz Valley (Cordillera Blanca, Peru), Earth Surf Process Landf, 43, 1373-1389, 10.1002/esp.4318, 2018b.
Muthusamy, M., Casado, M. R., Butler, D., and Leinster, P.: Understanding the effects of Digital Elevation Model resolution in urban fluvial flood modelling, Journal of Hydrology, 596, 10.1016/j.jhydrol.2021.126088, 2021.
NASA-JPL: NASADEM Merged DEM Global 1 arc second V001. Distributed by OpenTopography, Distributed by OpenTopography [dataset], https://doi.org/10.5069/G93T9FD9, 2021.
NCHM: Reassessment of Potentially Dangerous Glacial Lakes in Bhutan, National Centre for Hydrology and Meteorology, Royal Government of Bhutan, National Center for Hydrology and Meteorology, Royal Government of Bhutan, PO Box: 2017, Thimphu, Bhutan, 54, 2019a.
NCHM: Detailed assessment report on GLOF hazard from Thorthormi glacial lakes and asssociated glaciers, Thimphu, 2019b.
NCHM: Action Taken Report Thorthormi Flood Incident 30th October 2023, National Center for Meteorology and Hydrology, Thimphu, 17, 2023.
Nie, Y., Liu, Q., Wang, J., Zhang, Y., Sheng, Y., and Liu, S.: An inventory of historical glacial lake outburst floods in the Himalayas based on remote sensing observations and geomorphological analysis, Geomorphology, 308, 91-106, 10.1016/j.geomorph.2018.02.002, 2018.
Nie, Y., Deng, Q., Pritchard, H. D., Carrivick, J. L., Ahmed, F., Huggel, C., Liu, L., Wang, W., Lesi, M., Wang, J., Zhang, H., Zhang, B., Lü, Q., and Zhang, Y.: Glacial lake outburst floods threaten Asia's infrastructure, Science Bulletin, 10.1016/j.scib.2023.05.035, 2023.
Obu, J., Westermann, S., Bartsch, A., Berdnikov, N., Christiansen, H. H., Dashtseren, A., Delaloye, R., Elberling, B., Etzelmüller, B., Kholodov, A., Khomutov, A., Kääb, A., Leibman, M. O., Lewkowicz, A. G., Panda, S. K., Romanovsky, V., Way, R. G., Westergaard-Nielsen, A., Wu, T., Yamkhin, J., and Zou, D.: Northern Hemisphere permafrost map based on TTOP modelling for 2000–2016 at 1 km2 scale, Earth-Science Reviews, 193, 299-316, 10.1016/j.earscirev.2019.04.023, 2019.
Pudasaini, S. P.: A general two-phase debris flow model, Journal of Geophysical Research: Earth Surface, 117, 10.1029/2011jf002186, 2012.
Pudasaini, S. P. and Krautblatter, M.: A two-phase mechanical model for rock-ice avalanches, Journal of Geophysical Research: Earth Surface, 119, 2272-2290, 10.1002/2014jf003183, 2014a.
Pudasaini, S. P. and Krautblatter, M.: A two-phase mechanical model for rock-ice avalanches, Journal of Geophysical Research: Earth Surface, 119, 2272-2290, 10.1002/2014jf003183, 2014b.
Pudasaini, S. P. and Mergili, M.: A Multi-Phase Mass Flow Model, Journal of Geophysical Research: Earth Surface, 124, 2920-2942, 10.1029/2019jf005204, 2019.
Rinzin, S., Zhang, G., and Wangchuk, S.: Glacial Lake Area Change and Potential Outburst Flood Hazard Assessment in the Bhutan Himalaya, Frontiers in Earth Science, 9, 10.3389/feart.2021.775195, 2021.
Rinzin, S., Zhang, G., Sattar, A., Wangchuk, S., Allen, S. K., Dunning, S., and Peng, M.: GLOF hazard, exposure, vulnerability, and risk assessment of potentially dangerous glacial lakes in the Bhutan Himalaya, Journal of Hydrology, 619, 10.1016/j.jhydrol.2023.129311, 2023.

Rounce, D., Watson, C., and McKinney, D.: Identification of Hazard and Risk for Glacial Lakes in the Nepal Himalaya Using Satellite Imagery from 2000–2015, Remote Sens-Basel, 9, 10.3390/rs9070654, 2017.
Rounce, D. R., McKinney, D. C., Lala, J. M., Byers, A. C., and Watson, C. S.: A new remote hazard and risk assessment framework for glacial lakes in the Nepal Himalaya, Hydrology and Earth System Sciences, 20, 3455-3475, 10.5194/hess-20-3455-2016, 2016.
Saksena, S. and Merwade, V.: Incorporating the effect of DEM resolution and accuracy for improved flood inundation mapping, Journal of Hydrology, 530, 180-194, 10.1016/j.jhydrol.2015.09.069, 2015.
Saltelli, A., Tarantola, S., Campolongo, F., and Ratto, M.: Sensitivity analysis in practice: a guide to assessing scientific models, Wiley Online Library2004.
Sattar, A., Haritashya, U. K., Kargel, J. S., Leonard, G. J., Shugar, D. H., and Chase, D. V.: Modeling lake outburst and downstream hazard assessment of the Lower Barun Glacial Lake, Nepal Himalaya, Journal of Hydrology, 598, 10.1016/j.jhydrol.2021.126208, 2021a.
Sattar, A., Goswami, A., Kulkarni, A. V., Emmer, A., Haritashya, U. K., Allen, S., Frey, H., and Huggel, C.: Future Glacial Lake Outburst Flood (GLOF) hazard of the South Lhonak Lake, Sikkim Himalaya, Geomorphology, 388, 10.1016/j.geomorph.2021.107783, 2021b.
Sattar, A., Allen, S., Mergili, M., Haeberli, W., Frey, H., Kulkarni, A. V., Haritashya, U. K., Huggel, C., Goswami, A., and Ramsankaran, R.: Modeling Potential Glacial Lake Outburst Flood Process Chains and Effects From Artificial Lake-Level Lowering at Gepang Gath Lake, Indian Himalaya, Journal of Geophysical Research: Earth Surface, 128, 10.1029/2022jf006826, 2023.
Sattar, A., Cook, K. L., Rai, S. K., Berthier, E., Allen, S., Rinzin, S., Van Wyk de Vries, M., Haeberli, W., Kushwaha, P., Shugar, D. H., Emmer, A., Haritashya, U. K., Frey, H., Rao, P., Gurudin, K. S. K., Rai, P., Rajak, R., Hossain, F., Huggel, C., Mergili, M., Azam, M. F., Gascoin, S., Carrivick, J. L., Bell, L. E., Ranjan, R. K., Rashid, I., Kulkarni, A. V., Petley, D., Schwanghart, W., Watson, C. S., Islam, N., Gupta, M. D., Lane, S. N., and Bhat, S. Y.: The Sikkim flood of October 2023: Drivers, causes and impacts of a multihazard cascade, Science, 0, eads2659, doi:10.1126/science.ads2659, 2025.
Schneider, D., Huggel, C., Cochachin, A., Guillén, S., and García, J.: Mapping hazards from glacier lake outburst floods based on modelling of process cascades at Lake 513, Carhuaz, Peru, Advances in Geosciences, 35, 145-155, 10.5194/adgeo-35-145-2014, 2014.
Schumann, G. J. P. and Bates, P. D.: The Need for a High-Accuracy, Open-Access Global DEM, Frontiers in Earth Science, 6, 10.3389/feart.2018.00225, 2018.
Shean, D.: High Mountain Asia 8-meter DEM mosaics derived from optical imagery, version 1, Boulder, CO: NASA National Snow and Ice Data Center Distributed Active Archive Center. doi, 10, 002214309790152555, 2017a.
Shean, D.: High Mountain Asia 8-meter DEM mosaics derived from optical imagery (1), NASA National Snow and Ice Data Center Distributed Active Archive Center [dataset], 2017b.
Shean, D. E., Alexandrov, O., Moratto, Z. M., Smith, B. E., Joughin, I. R., Porter, C., and Morin, P.: An automated, open-source pipeline for mass production of digital elevation models (DEMs) from very-high-resolution commercial stereo satellite imagery, ISPRS Journal of Photogrammetry and Remote Sensing, 116, 101-117, 10.1016/j.isprsjprs.2016.03.012, 2016.
Shrestha, F., Steiner, J. F., Shrestha, R., Dhungel, Y., Joshi, S. P., Inglis, S., Ashraf, A., Wali, S., Walizada, K. M., and Zhang, T.: HMAGLOFDB v1.0 – a comprehensive and version controlled database of glacier lake outburst floods in high mountain Asia, Earth Syst. Sci. Data Discuss., 2023, 1-28, 10.5194/essd-2022-395, 2023.
Shugar, D. H., Burr, A., Haritashya, U. K., Kargel, J. S., Watson, C. S., Kennedy, M. C., Bevington, A. R., Betts, R. A., Harrison, S., and Strattman, K.: Rapid worldwide growth of glacial lakes since 1990, Nature Climate Change, 10, 939-945, 10.1038/s41558-020-0855-4, 2020.
Shugar, D. H., Jacquemart, M., Shean, D., Bhushan, S., Upadhyay, K., Sattar, A., Schwanghart, W., McBride, S., de Vries, M. V. W., Mergili, M., Emmer, A., Deschamps-Berger, C., McDonnell, M., Bhambri, R., Allen, S., Berthier, E., Carrivick, J. L., Clague, J. J., Dokukin, M., Dunning, S. A., Frey, H., Gascoin, S., Haritashya, U. K., Huggel, C., Kääb, A., Kargel, J. S., Kavanaugh, J. L., Lacroix, P., Petley, D.,

Rupper, S., Azam, M. F., Cook, S. J., Dimri, A. P., Eriksson, M., Farinotti, D., Fiddes, J., Gnyawali, K. R., Harrison, S., Jha, M., Koppes, M., Kumar, A., Leinss, S., Majeed, U., Mal, S., Muhuri, A., Noetzli, J., Paul, F., Rashid, I., Sain, K., Steiner, J., Ugalde, F., Watson, C. S., and Westoby, M. J.: A massive rock and ice avalanche caused the 2021 disaster at Chamoli, Indian Himalaya, Science, 373, 300, 10.1126/science.abh4455, 2021.
Somos-Valenzuela, M. A., McKinney, D. C., Byers, A. C., Rounce, D. R., Portocarrero, C., and Lamsal, D.: Assessing downstream flood impacts due to a potential GLOF from Imja Tsho in Nepal, Hydrology and Earth System Sciences, 19, 1401-1412, 10.5194/hess-19-1401-2015, 2015.
Taylor, C., Robinson, T. R., Dunning, S., Rachel Carr, J., and Westoby, M.: Glacial lake outburst floods threaten millions globally, Nature Communications, 14, 487, 10.1038/s41467-023-36033-x, 2023.
Thompson, I., Shrestha, M., Chhetri, N., and Agusdinata, D. B.: An institutional analysis of glacial floods and disaster risk management in the Nepal Himalaya, International Journal of Disaster Risk Reduction, 47, 10.1016/j.ijdrr.2020.101567, 2020.
Uuemaa, E., Ahi, S., Montibeller, B., Muru, M., and Kmoch, A.: Vertical Accuracy of Freely Available Global Digital Elevation Models (ASTER, AW3D30, MERIT, TanDEM-X, SRTM, and NASADEM), Remote Sens-Basel, 12, 10.3390/rs12213482, 2020.
Vilca, O., Mergili, M., Emmer, A., Frey, H., and Huggel, C.: The 2020 glacial lake outburst flood process chain at Lake Salkantaycocha (Cordillera Vilcabamba, Peru), Landslides, 18, 2211-2223, 10.1007/s10346-021-01670-0, 2021.
Wang, W., Yang, X., and Yao, T.: Evaluation of ASTER GDEM and SRTM and their suitability in hydraulic modelling of a glacial lake outburst flood in southeast Tibet, Hydrological Processes, 26, 213-225, 10.1002/hyp.8127, 2011.
Wang, X., Guo, X., Yang, C., Liu, Q., Wei, J., Zhang, Y., Liu, S., Zhang, Y., Jiang, Z., and Tang, Z.: Glacial lake inventory of high-mountain Asia in 1990 and 2018 derived from Landsat images, Earth System Science Data, 12, 2169-2182, 10.5194/essd-12-2169-2020, 2020.
Wang, Y., Hutter, K., and Pudasaini, S. P.: The Savage-Hutter theory: A system of partial differential equations for avalanche flows of snow, debris, and mud, ZAMM - Journal of Applied Mathematics and Mechanics / Zeitschrift für Angewandte Mathematik und Mechanik, 84, 507-527, 10.1002/zamm.200310123, 2004.
Watson, C. S., Carrivick, J., and Quincey, D.: An improved method to represent DEM uncertainty in glacial lake outburst flood propagation using stochastic simulations, Journal of Hydrology, 529, 1373-1389, 10.1016/j.jhydrol.2015.08.046, 2015.
Westoby, M. J., Glasser, N. F., Brasington, J., Hambrey, M. J., Quincey, D. J., and Reynolds, J. M.: Modelling outburst floods from moraine-dammed glacial lakes, Earth-Science Reviews, 134, 137-159, 10.1016/j.earscirev.2014.03.009, 2014.
Westoby, M. J., Brasington, J., Glasser, N. F., Hambrey, M. J., Reynolds, J. M., Hassan, M. A. A. M., and Lowe, A.: Numerical modelling of glacial lake outburst floods using physically based dam-breach models, Earth Surface Dynamics, 3, 171-199, 10.5194/esurf-3-171-2015, 2015.
Worni, R., Huggel, C., and Stoffel, M.: Glacial lakes in the Indian Himalayas--from an area-wide glacial lake inventory to on-site and modeling based risk assessment of critical glacial lakes, Sci Total Environ, 468-469 Suppl, S71-84, 10.1016/j.scitotenv.2012.11.043, 2013.
Worni, R., Stoffel, M., Huggel, C., Volz, C., Casteller, A., and Luckman, B.: Analysis and dynamic modeling of a moraine failure and glacier lake outburst flood at Ventisquero Negro, Patagonian Andes (Argentina), Journal of Hydrology, 444-445, 134-145, 10.1016/j.jhydrol.2012.04.013, 2012.
Zhang, G., Yao, T., Xie, H., Wang, W., and Yang, W.: An inventory of glacial lakes in the Third Pole region and their changes in response to global warming, Global and Planetary Change, 131, 148-157, 10.1016/j.gloplacha.2015.05.013, 2015.
Zhang, G., Bolch, T., Yao, T., Rounce, D. R., Chen, W., Veh, G., King, O., Allen, S. K., Wang, M., and Wang, W.: Underestimated mass loss from lake-terminating glaciers in the greater Himalaya, Nature Geoscience, 10.1038/s41561-023-01150-1, 2023a.

Zhang, T., Wang, W., and An, B.: Heterogeneous changes in global glacial lakes under coupled climate warming and glacier thinning, Communications Earth & Environment, 5, 10.1038/s43247-024-01544-y, 2024.
Zhang, T., Wang, W., An, B., and Wei, L.: Enhanced glacial lake activity threatens numerous communities and infrastructure in the Third Pole, Nature Communications, 14, 10.1038/s41467-023-44123-z, 2023b.
Zheng, G., Mergili, M., Emmer, A., Allen, S., Bao, A., Guo, H., and Stoffel, M.: The 2020 glacial lake outburst flood at Jinwuco, Tibet: causes, impacts, and implications for hazard and risk assessment, The Cryosphere Discuss., 2021, 1-28, 10.5194/tc-2020-379, 2021a.
Zheng, G., Allen, S. K., Bao, A., Ballesteros-Cánovas, J. A., Huss, M., Zhang, G., Li, J., Yuan, Y., Jiang, L., Yu, T., Chen, W., and Stoffel, M.: Increasing risk of glacial lake outburst floods from future Third Pole deglaciation, Nature Climate Change, 11, 411-417, 10.1038/s41558-021-01028-3, 2021b.